PET/MRI for Clinical Pediatric Oncologic Imaging

21

Maria Rosana Ponisio, Pooya Iranpour, Geetika Khanna, and Jonathan McConathy

Contents

21.1 Overview

PET/MRI has significant potential advantages over PET/CT for use in pediatric populations including decreasing radiation dose, reducing exposure to sedation and anesthesia, reducing the need for gadolinium-based MR contrast agents, and increasing convenience to children and their families through combining PET and MRI acquisition into a single imaging session. PET/MRI is a clinical reality and is in routine use at a number of academic centers as well as in a few private practices with some centers performing pediatric imaging. Although promising, PET/MRI

M.R. Ponisio • P. Iranpour • G. Khanna
Department of Radiology, Washington University in St. Louis, St. Louis, MO, USA

J. McConathy (✉)
Division of Molecular Imaging and Therapeutics, Department of Radiology, University of Alabama at Birmingham, Birmingham, AL, USA
e-mail: jmcconathy@uabmc.edu

A. Iagaru et al. (eds.), *PET/MRI in Oncology*,
https://doi.org/10.1007/978-3-319-68517-5_21

for pediatric oncology faces significant challenges including the high cost and relatively limited availability of PET/MRI systems, the lack of standardization across centers, limited evidence demonstrating the superiority of PET/MRI compared to PET/CT and other imaging modalities, and variable institutional utilization of PET and whole-body MR imaging in the diagnostic evaluation of children with cancer.

This chapter provides an overview of current and possible future uses of PET/MRI for clinical oncologic imaging in children. PET/MRI has great potential for basic and translational research in children and adults, but the focus of this chapter is on the use of PET/MRI in routine patient care. The strengths and limitations of this technology and the available PET tracers for specific applications in pediatric oncology are key topics discussed here.

21.2 PET Tracers Relevant to Pediatric Oncology

PET uses compounds labeled with positron-emitting radionuclides to form three-dimensional tomographic images that reflect functional, metabolic, or biochemical information. The structure and pharmacologic properties of the PET tracer determine the biological information obtained through PET imaging, and a very wide range of targets including biological transporters, metabolic pathways, enzymes, and receptors have been successfully targeted with PET. The high sensitivity and molecular specificity of PET make this modality very valuable in oncologic imaging for both routine clinical and research applications. The physical properties of the positron-emitting radionuclide use in a PET tracer can affect resolution and dosimetry, and for some radionuclide the scanner settings and image reconstruction should be adjusted to obtain optimal image quality. An important limitation of PET is the low resolution compared to anatomic techniques such as CT and MRI. Hybrid imaging with PET/CT and PET/MRI allows collection of anatomic and molecular information in a single study.

The most widely used PET tracer for adult and pediatric oncologic imaging is the glucose analogue, 2-deoxy-2-[^{18}F]fluoro-D-glucose (FDG). Most of the PET/MRI studies discussed in this chapter utilize FDG as the PET tracer. FDG is transported into cells via glucose transporters and then phosphorylated by hexokinase enzymes, trapping FDG inside the cell [1]. Many cancer cells have upregulated glycolytic metabolism of glucose (i.e., conversion of glucose to lactate) even in the presence of adequate levels of oxygen to perform oxidative phosphorylation [2, 3]. This phenomenon is known as aerobic glycolysis (the Warburg effect) and is the basis for the utility of FDG-PET for detecting and assessing response to therapy in a wide range of human cancers. One of the limitations of FDG is the high uptake in inflammatory lesions which can lead to false-positive studies for malignancy. FDG also has high physiologic uptake in the brain and moderate uptake in the liver as well as excretion in the urine; this normal biodistribution can obscure malignant lesions in these locations. The uptake of FDG can be low in certain tumors with low glycolytic activity such as mucinous tumor histologies and low-grade neoplasms, leading to false negatives. Finally, FDG-PET evaluates only one aspect of cancer biology, and other

PET tracers may have better sensitivity and specificity for certain cancers and can provide biological information relevant to prognosis and therapy not available with FDG.

A number of PET tracers other than FDG have been developed and have potential utility for PET/MRI in pediatric oncology. However, there is limited data regarding the diagnostic utility of these tracers in children and very little data comparing PET/MRI to PET/CT with non-FDG-PET tracers. The PET tracer sodium [^{18}F]fluoride (NaF) is used for skeletal scintigraphy and is very sensitive for detecting blastic metastases as well as other processes causing increased turnover of the mineralized bone. Radiolabeled amino acids targeting system L amino acid transport can complement MRI for the evaluation of brain tumors by providing better assessment of non-enhancing regions in glioma and increasing the accuracy of assessment of brain tumors after therapy [4–6]. Peptide-based somatostatin receptor ligands labeled with Ga-68 include DOTATOC, DOTATATE, and DOTANOC which are particularly useful for tumors that express somatostatin receptors on their cell surface such as well-differentiated neuroendocrine tumors and meningiomas [7–10]. These somatostatin receptor imaging agents may have roles in evaluating neuroblastoma and pheochromocytoma in children and can also be used for therapy when they are labeled with therapeutic radionuclides such as Lu-177 or Y-90 [11, 12]. The amino acid 3,4-dihydroxy-6-[^{18}F]fluoro-D-phenylalanine (FDOPA) may also be useful for neuroendocrine tumors and for preoperative planning in children with congenital hyperinsulinemia [13–16].

There is also the potential to convert single photon computed tomography (SPECT) agents into PET agents by replacing I-123 or I-131 which are not suitable for PET with the positron-emitting radionuclide I-124. For example, sodium [^{124}I] iodide could be used for imaging differentiated thyroid cancer [17–19], and *meta*-iodobenzylguanidine (MIBG) labeled with I-124 could be used for PET imaging of neuroblastoma [20, 21]. However, these PET analogues of routinely used SPECT agents are not widely available, and very little data regarding their efficacy in pediatric patients are available.

21.3 Pediatric PET/MRI Protocols and Workflows

The available data from pediatric PET/MRI studies and the larger body of work in adult PET/MRI studies suggest that FDG-PET/MRI is equivalent to FDG-PET/CT in terms of whole-body staging for most cancers [22–27]. Many clinical PET/MRI studies are performed when both whole-body staging with PET and local tumor or organ staging with MRI are needed. In some anatomic regions such as the brain, liver, pelvis, and bone marrow, MRI provides superior soft tissue contrast and sensitivity to CT even in the absence of gadolinium-based MR contrast agents. In children and young adults with potentially curable cancers, PET/MRI decreases exposure to ionizing radiation by replacing CT with MRI as discussed in more detail later in this chapter.

In our practice, PET/MRI in the pediatric population is performed chiefly for the following indications: (1) dose reduction in pediatric patients who need a whole-body

PET alone, such as lymphoma; (2) pediatric patients who need a whole-body PET and a dedicated regional MRI, such as brain tumors, sarcomas, and neuroblastoma; and (3) pediatric patients who need a brain PET and MRI for epilepsy evaluation. Protocols in PET/MRI for adults and children typically are modified from standard dedicated MRI to maintain patient throughput and tolerance. The protocols for clinical PET/MRI are evolving, and this section reflects our experience as well as reports and protocols from other institutions. The aim of the modified MRI protocol should be that the entire scan (whole-body PET, whole-body MRI for attenuation correction/localization, and dedicated regional MRI as needed) can be completed within less than 60 min. If regional dedicated MRI is not needed, we aim to complete the whole-body simultaneous PET/MRI in around 30 min. Using this approach, it is feasible to scan children as young as 8 years old without sedation. Table 21.1 gives an example of a modified MRI protocol performed in the simultaneous PET/MRI setting. The whole-body portion is typically performed first in case the study must be terminated early, maximizing the chance the radiopharmaceutical administration results in a diagnostic study. Although not optimal, the regional MRI can be performed separately if the entire whole-body and regional PET/MRI study cannot be completed.

When performing whole-body PET-MRI, multiple phase array coils should be used as opposed to the body coil to provide adequate signal-to-noise ratio. The patient's arms are placed by their side and included in the field of view for attenuation correction and whole-body imaging. If dedicated imaging of the head is not needed, the head coil can be left off, especially in claustrophobic patients. The scan starts with whole-body simultaneous acquisition of PET data, two-point Dixon sequences, single-shot fast spin echo (SSFSE) imaging, and inversion recovery or diffusion-weighted imaging. We typically acquire these sequences in the axial plane

Table 21.1 Example of a modified liver MRI protocol for detection of hepatic metastases used in pediatric simultaneous PET/MRI

Standard liver MRI protocol	Modified liver MRI protocol
Three-plane localization	Part of whole-body acquisition
Coronal single-shot fast spin echo	Omitted
Axial single-shot fast spin echo	Part of whole-body acquisition
Coronal steady-state free procession (e.g., true FISP. FIESTA)	Omitted
Axial coherent gradient echo	Omitted
Axial in/opposed phase	Part of whole-body acquisition
Axial T2 fast spin echo fat saturated	Axial T2 fast spin echo fat saturated
Axial diffusion weighted (*b*-values 50, 400, 800 mm/s^2)	Axial diffusion weighted (*b*-values 50, 400, 800 mm/s^2)
Pre-contrast T1 ultrafast gradient echo (e.g., VIBE, LAVA)	Pre-contrast T1 ultrafast gradient echo (e.g., VIBE, LAVA)
Post-contrast T1 ultrafast gradient-echo dynamic × 3	Post-contrast T1 ultrafast gradient-echo dynamic × 3

Some of the standard liver MRI protocol sequences are included in the whole-body MRI acquisition, while others are omitted in the modified liver MRI protocol to reduce the overall length of the examination without reducing detection of metastases

and reconstruct and compose images in the coronal plane to get whole-body images. Acquiring these images in a contiguous rather than interleaved fashion allows reconstruction without blurring or stair-stepping artifact. The scan time at each station is around 3 min, with a z-axis coverage of 25 cm/station. So, whole-body imaging in a typical teenager is achieved in six stations, resulting in an active scanning time of ~20 min for the basic whole-body PET/MRI scan.

The two-point Dixon sequence automatically generates four image sets: in phase, out of phase, fat only, and water only. These are used to create the MR-based attenuation correction map that is applied to the PET data. Studies in adults indicate that the image sets derived from the Dixon sequence can provide similar anatomic localization as the non-contrast CT portion of FDG-PET/CT studies [24, 28]. The in phase/out of phase images should be evaluated for evidence of liver iron deposition, a common problem in pediatric cancer survivors [29]. The water-only sequence is the equivalent of a pre-contrast T1-weighted fat-saturated image and can provide good anatomic detail. The SSFSE sequence is optional but is useful for providing an overview of anatomy and for localization. These are acquired free breathing, without navigation, when performed simultaneous with acquisition of the PET data. Diffusion-weighted imaging is typically performed with three different *b*-values, 50, 400–500, and 800–1000 mm/s^2, which are then used to generate the apparent diffusion coefficient (ADC) map. The low *b*-value images have the most T2 weighting and can function as T2 fat-saturated/inversion recovery sequence, which is useful for both lesion detection and localization. Lesion characterization as benign vs. malignant is best performed on the high *b*-value images in correlation with the ADC map, keeping in mind that several benign lesions (such as focal nodular hyperplasia in the liver) can show diffusion restriction [30].

After the whole-body acquisition, dedicated anatomic imaging of the primary site for locoregional staging or specific metastatic site in question (such as the liver) is performed without and with intravenous contrast. There is an increasing body of literature in the pediatric setting that has questioned the need for the routine use of intravenous contrast in follow-up of pediatric cancer patients [31]. The avoidance of intravenous contrast can help decrease the duration of the scan, avoid the unknown long-term consequences of intracranial gadolinium deposition, and most importantly replace the use of gadolinium-based contrast agents with organ-/tumor-specific contrast agents—such as ferumoxytol for the evaluation of lymph nodes [32–34]. Our experience has been that intravenous contrast is needed for evaluation of visceral metastasis, especially in organs with relatively high physiologic FDG uptake such as the brain, liver, and spleen. Use of hepatocyte-specific contrast agents with delayed imaging obtained in the hepatocyte phase can demonstrate liver metastasis with high sensitivity as seen in Fig. 21.1.

There are several challenges with hybrid PET/MRI scanning that must be considered. The long duration of scans compared to PET/CT may not be tolerated by some patients and can negatively impact patient throughput. The current clinically available PET/MRI systems have 3 T magnets which can lead to encountering specific absorption rate (SAR) limits especially when scanning smaller children and increased susceptibility artifacts such as from bowel gas/surgical clips compared to

MRI at 1.5 T. In addition, hybrid PET/MRI remains less sensitive than CT for the detection of subcentimeter pulmonary metastasis [35–37], so dedicated chest CT is still needed in pediatric tumors that are known to metastasize to the lungs. The use of ultrashort echo time sequences allows better delineation of pulmonary nodules compared with conventional dual-echo gradient-echo sequences and may in part overcome this limitation of PET/MRI [38].

For patients who need a chest CT evaluation of pulmonary metastasis such as sarcoma patients, a non-contrast chest CT is performed before or after the PET/MRI to avoid dependent atelectasis in the lungs. Intravenous contrast is not given for this CT as mediastinal and hilar nodes can be evaluated by PET/MRI and a non-contrast chest CT can be performed without sedation in the vast majority of children, irrespective of age. The nuclear medicine technologist and MRI technologist work in conjunction to screen and prep the patient, while scanning is performed primarily by the MRI technologist. In our institution, joint reading is performed for all PET/MRI scans by nuclear medicine physicians and radiologists. If a dedicated MRI is performed, two reports are generated; however, in patients who undergo the PET/MRI in lieu of a PET/CT with basic whole-body MRI sequences only, only one report is generated by the nuclear medicine physicians.

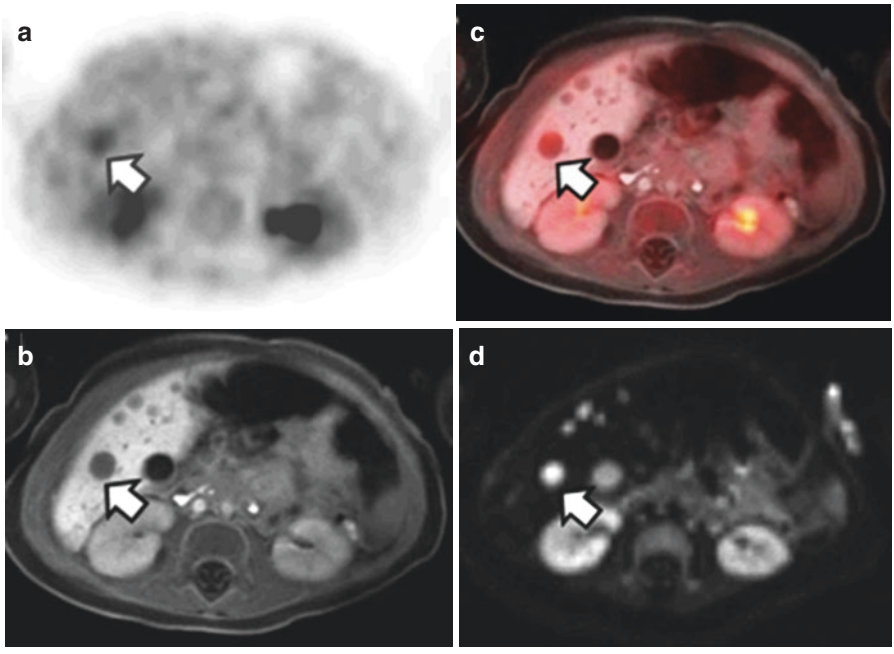

Fig. 21.1 FDG-PET/MRI performed in a 4-month-old girl after recent resection of a right adrenal neuroblastoma. During surgery, liver metastases were discovered that were not well seen on preoperative CT. Whole body FDG PET/MRI shows hepatic lesions which are FGD-avid (**a**), hypoenhancing on the hepatobiliary phase MRI (**b**, **f**) and demonstrates restricted diffusion (**d**). Smaller lesions were not identified on FDG-PET but are well visualized on the hepatobiliary phase and DWI (**d**, **h**). (**a**, **e**) FDG-PET; (**b**, **f**) hepatobiliary phase MRI; (**c**, **g**) fused PET/MRI; (**d**, **h**) Diffusion weighted imaging (DWI); Maximum intensity projection (MIP) is also shown (**i**)

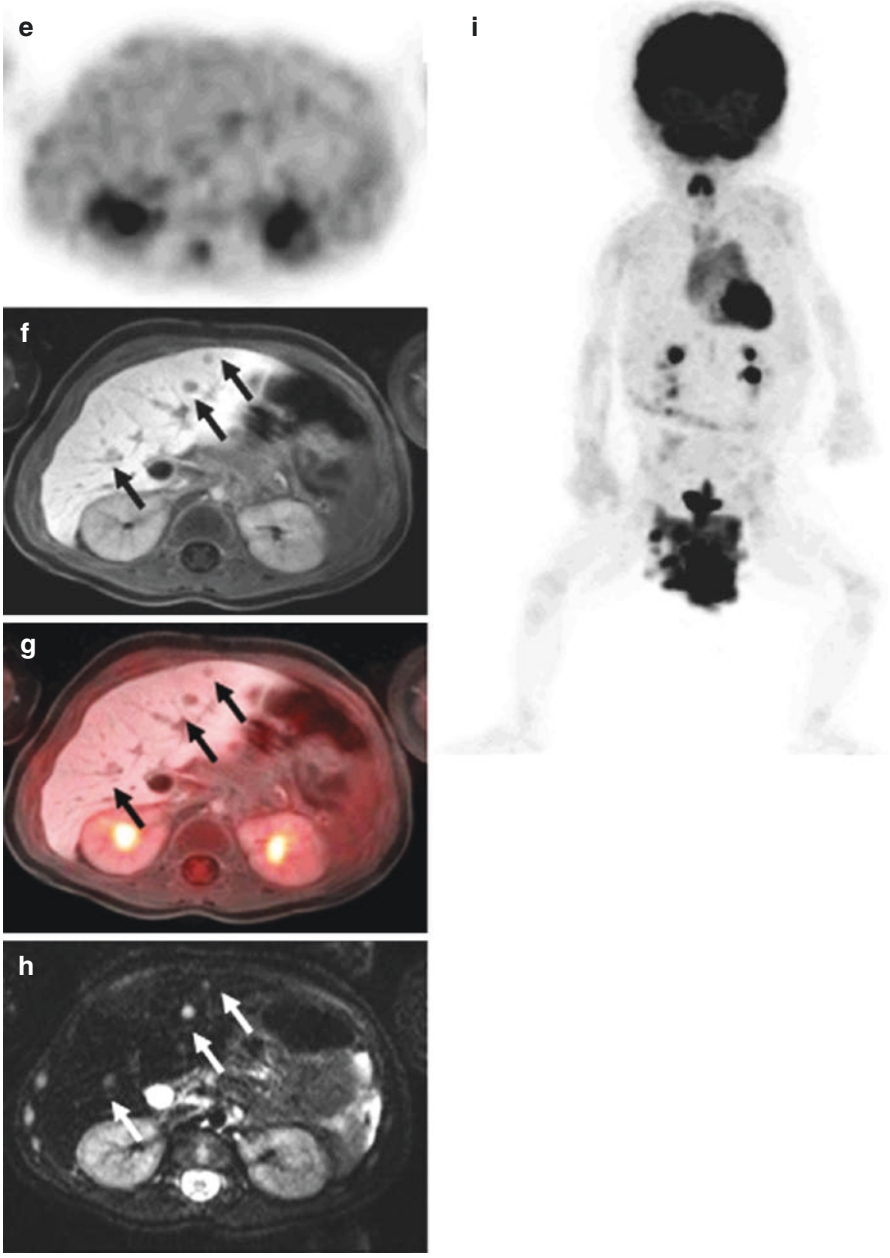

Fig. 21.1 (continued)

21.4 Dose Reduction with PET/MRI

In recent years, there have been major initiatives aimed at reducing ionizing radiation dose from medical imaging. These dose reduction efforts such as the Image Gently campaign for pediatric patients are motivated by the increased utilization of diagnostic imaging combined with the small increased risk of cancer incidence and mortality related to ionizing radiation exposure based on the linear no-threshold model [39]. A general principle that applies to all diagnostic imaging techniques that utilize ionizing radiation is to impart the minimum patient dose needed to answer the clinical question.

PET/MRI has the potential to reduce the radiation dose compared to PET/CT without reducing diagnostic imaging quality by substituting MRI for CT and by reducing the dosage of the PET tracer. However, PET agent still confers a substantial portion of the patient dose, and dose reduction by using PET/MRI instead of PET/CT for [^{18}F]FDG studies ranges from approximately 39 to 73% based on published comparisons [22, 23, 40, 41]. The variability in dose reduction is in large part due to different PET/CT hardware and CT protocols across centers.

Comparisons of the relative radiation exposure from different imaging techniques (e.g., PET compared to CT) are typically expressed as the effective dose (ED) with units of mSv or rem. The ED is a whole-body dose that accounts for both the radiation weighting factor and the tissue weighting factor, which defines the radiosensitivity of each organ that is involved [42, 43]. The ED is equal to what the whole-body equivalent dose of ionizing radiation would be if emitted and/or transmitted uniformly. The ED related to the amount of administered activity from the PET tracer increases with younger ages. For example, the ED related to [^{18}F]FDG is 95 μSv/MBq for a 1-year-old child, 37 μSv/MBq for a 10-year-old child, and 19 μSv/MBq for an adult [44].

The biodistribution, half-life, and emission profile of positron-emitting radionuclide used for labeling affect the dosimetry of a PET tracer. Factors that increase the ED in PET studies include high and persistent tracer accumulation in radiosensitive organs, long physical half-life of the radionuclide, and high fractions of emissions resulting from nuclear decay (e.g., gamma rays) other than positrons. For clinical PET studies, using a different PET radionuclide is generally not an option, so reducing the administered dosage of the PET tracer is the primary method for reducing radiation dose to the patient from the PET component of the study.

Patient dose from CT depends on the tube voltage (kV or kVp), the milliampere-seconds (mA-S), the gantry pitch, and the total beam width [45]. These parameters are often adjusted in PET/CT examinations to impart a lower patient dose than a typical diagnostic CT but still provide substantial structural and morphological information that can aid in the interpretation of the PET findings. The CT dose can be lowered further if only attenuation correction is needed, but only limited structural and morphological information can be obtained from these types of CT studies. The overall estimated increased risk of cancer associated with diagnostic imaging is low compared to the lifetime risk of cancer but is not zero [39, 46]. Because the additional risk for cancer associated with PET/CT is small compared to the overall risk of developing cancer, PET/CT will remain a viable modality for pediatric oncologic imaging even if PET/MRI becomes more widely available.

PET/MRI eliminates the CT portion of the examination while still providing attenuation correction and anatomical localization, and there are additional opportunities for dose reduction [23]. The patient dose related to the PET radiopharmaceutical can be reduced through longer image acquisition times and/or higher sensitivity PET detectors which can reduce the dosage of radiopharmaceutical required [22, 47–49]. Longer PET acquisition times to match that of the MRI examination can also be used to compensate for smaller dosages of the PET tracer. However, prolonged image acquisition must be balanced with patient tolerance as longer imaging times may result in degraded imaging quality due to patient's motion and increased anesthesia time in younger patients.

21.5 Specific Applications of PET/MRI in Pediatric Oncology

21.5.1 Lymphoma

Lymphoma represents 12% of all malignancy in the pediatric population, and of these 40% are Hodgkin lymphomas (HL) [50]. Nodular sclerosis is the most common classical HL subtype occurring prevalently in adolescents. The most common sites involved by HL include mediastinal, cervical, and axillary lymph nodes. Non-Hodgkin lymphoma (NHL) accounts for 60% of childhood lymphomas and has its peak incidence at the age of 7 years. In the pediatric population, NHL is most often an aggressive systemic disease defined by mature B cell immunophenotype. The most common pediatric NHL is Burkitt lymphoma and B cell lymphoblastic lymphoma which represent 40–50% of cases. The classic presentation of lymphoblastic lymphomas, a nodal predominant form of acute lymphoblastic leukemia, is characterized by a large mediastinal mass and infiltration of the spleen, bone marrow, central nervous system, and peripheral lymph nodes. Low-grade NHL such as follicular and mantle cell lymphoma occur in children but are less common than in adults.

The majority of children with lymphoma have a good prognosis, with long-term survival rates >80% following treatment with chemotherapy or in combination with radiotherapy [51–53]. However, survivors of lymphoma are at high risk of second cancers which have been linked to the radiation field. The most common second malignancies include breast cancer in girls, followed by thyroid and gastrointestinal cancer, leukemia, and soft tissue sarcoma [54–56]. Additional side effects include impaired fertility, particularly in boys secondary to cumulative doses of alkylating agents, and treatment-associated cardiovascular disease [57]. Thus, there has been a shift in treatment paradigm, with emphasis on reducing iatrogenic toxicity and late side effects of chemotherapy in this population with increasing life expectancy. This has placed increased emphasis on diagnostic imaging to provide accurate information regarding the staging and response assessment for correct stratification and treatment management.

The role of whole-body MRI (WBMRI) has gained increased relevance for the evaluation of children with lymphoma for initial staging, monitoring treatment, and evaluation of treatment-related side effects, including corticoid-related osteonecrosis, which is an important cause of morbidity [58–60]. WBMRI has the advantages of not using ionizing radiation and providing high soft tissue contrast; however, one

key limitation is the lack of ability to distinguish between benign and malignant lymph nodes, even with the combination of diffusion-weighted imaging and anatomical criteria [61, 62]. A recent study in adult lymphoma patients [63] reported that whole-body diffusion-weighted MRI (WB-DW-MRI), which allowed for calculation of apparent diffusion coefficients (ADC), showed an inferior performance than that of FDG-PET/CT/MRI especially for staging, distinction of nodal and extra-nodal disease, and differentiation of high-grade and low-grade lymphoma.

FDG-PET/CT is a well-established imaging modality for staging and therapy response assessment on pediatric lymphoma patients. The majority of aggressive lymphoma subtypes demonstrate high FDG uptake, with the exception of extra-nodal marginal zone lymphoma and small lymphocytic lymphoma [64]; however, lower-grade lymphomas rarely present in pediatric patients. Accurate initial staging is crucial to define treatment, including intensity of chemotherapy and extension of radiation fields, in order to avoid unnecessary treatment-related side effects. FDG-PET/CT shows markedly greater sensitivity, specificity, and accuracy (95.9%, 99.7%, and 99.6%, respectively) compared with conventional imaging modalities (70.1%, 99.0%, and 98.3%, respectively). Additionally, several studies have reported that FDG-PET/CT imaging changed patient management in 12–50% of the cases [65–67].

In response assessment, FDG-PET has shown high specificity, sensitivity, and negative predictive value (NPV), with various studies concluding that NPV is a better guide of favorable prognosis than positive predictive value (PPV) [68, 69]. The role of NPV in patient management is important, providing a predictor for decreasing therapy intensity to reduce the potential incidence of toxicity in good responders. A significant advantage of PET over conventional imaging is the ability to distinguish residual active tumor from fibrosis/scarring. Responder patients show residual morphological abnormalities, most commonly persistent soft tissue mass with lack of increased FDG activity consistent with treated, nonviable tumor. An example of FDG-PET/MRI and FDG-PET/CT in Hodgkin lymphoma is shown in Fig. 21.2.

PET/MRI has been gaining acceptance in pediatric lymphoma. Table 21.2 summarizes the results of selected recent publications. The limited data on pediatric patients have demonstrated that FDG-PET/MRI is feasible in pediatric patients and provides similar diagnostic performance compared to standard of care FDG-PET/CT [70] with substantial reduction in radiation exposure (range 39–73%) [23, 40, 71], by eliminating the CT component of PET/CT. This is especially important in this population with potentially curable disease, where serial imaging is required during treatment monitoring and/or at completion of therapy. The study by Schafer et al. [23] performed on pediatric cancer patients (lymphoma = 7/14) showed that PET/MRI identified additional findings compared with PET/CT, including malignant bone marrow and renal infiltration and a soft issue metastasis [23].

We recommend that DWI be a standard sequence in whole-body PET/MRI protocols in pediatric oncology, in agreement with prior publications [72, 73]. Restricted diffusion suggests increased cellularity and a change in the nuclear-cytoplasmic ratio and therefore suggests the possibility to identify additional lesions, in particular extra-nodal lymphomatous involvement of the liver, spleen, and kidneys.

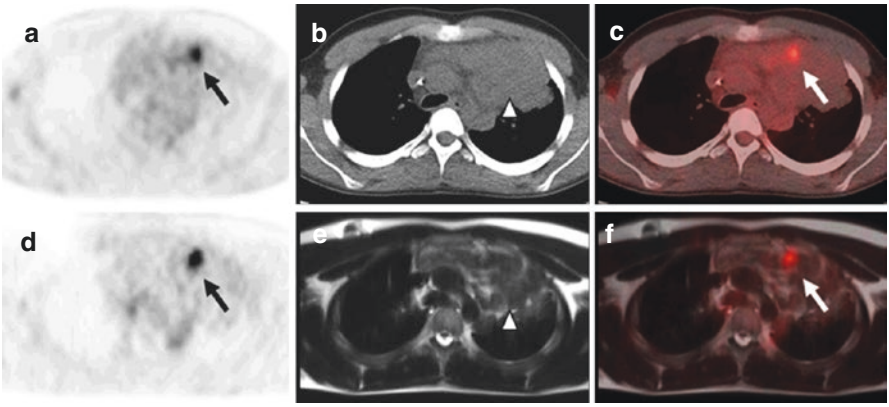

Fig. 21.2 Comparison of simultaneous FDG-PET/MRI with FDG-PET/CT in an 18-year-old male with large B-cell lymphoma for distinguishing fibrosis from viable lymphoma. The PET/MRI was performed immediately following the PET/CT using the same dose of FDG. FDG-PET/CT (**a**–**c**) and simultaneous whole body FDG-PET/MRI (**d**–**f**) demonstrate a large anterior mediastinum soft tissue mass (*arrow heads*) with a focus of increased FDG activity (*arrows*) suspicious for viable tumor. The remaining mass does not demonstrates increased FDG metabolic activity and likely represents scarring/fibrosis (*arrow head*). (**a**) FDG-PET from PET/CT acquisition; (**b**) CT mediastinal window; (**c**) fused FDG-PET/CT; (**d**) FDG-PET from PET/MRI acquisition; (**e**) T2 single shot fast spin echo; (**f**) fused FDG-PET/MRI

Table 21.2 Summary of selected studies evaluating the diagnostic utility of FDG-PET/MRI for pediatric lymphoma

Study	Number of patients	Average dose reduction	Major findings
Kirchner et al. [75]	12	Not reported	• FDG-PET/MRI was superior to whole-body DWI
			• MR contrast and DWI did not improve diagnostic accuracy of FDG-PET/MRI
Sher et al. [41]	25	45%	• FDG-PET/MRI was similar to PET/CT for
			– Lesion detection and classification
			– Ann Arbor staging
			– FDG uptake strongly correlated with PET/CT
Schafer et al. [23]	18	73%	• FDG-PET/MRI is clinically feasible
			• Equivalent rates of lesion detection to PET/CT
			• CT examination of the thorax might be necessary
Ponisio et al. [40]	8	39%	• FDG-PET/MRI is clinically feasible
			• FDG-PET/MRI was similar to PET/CT for
			– Lesion detection
			– SUV measurements

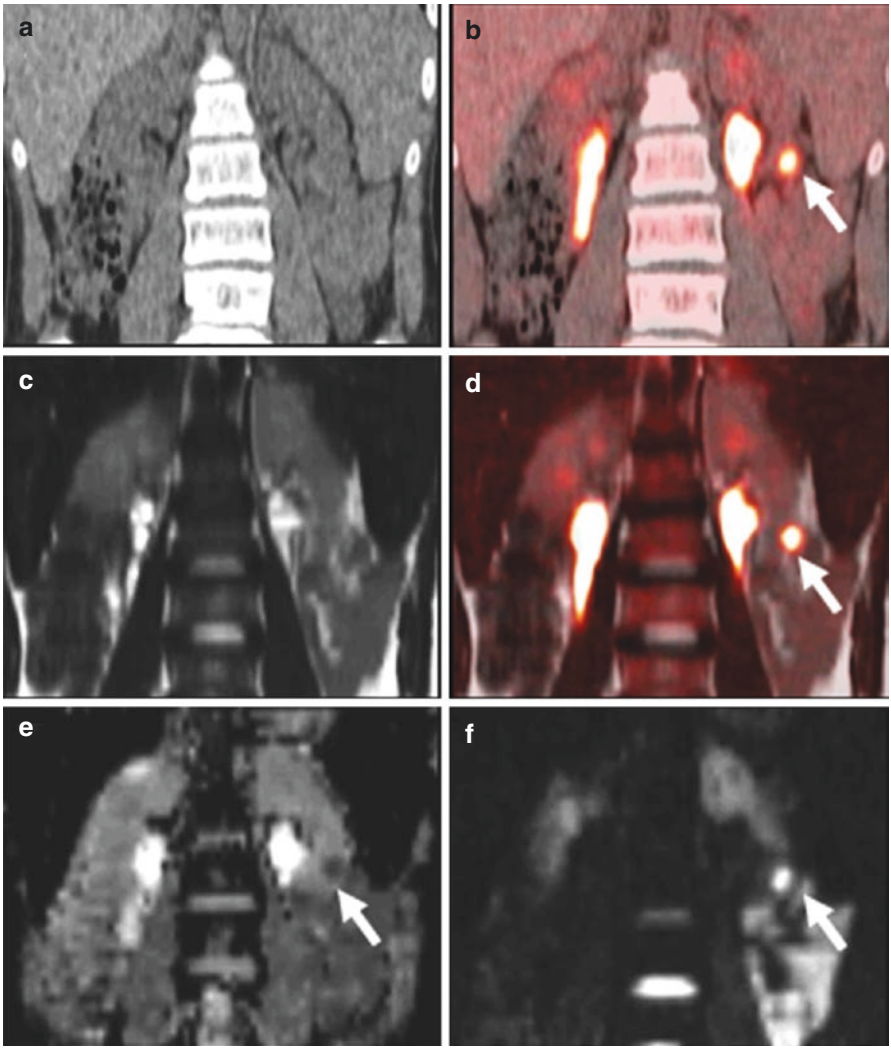

Fig. 21.3 17-year-old male with diffuse large B-cell lymphoma with focal left renal involvement. Restricted diffusion seen on DWI (**f**, *white arrow*) allowed better identification of the renal lesion and differentiation from excreted FDG in the collecting system. The lesion is not well identified on non-contrast CT (**a**) or T2 single shot fast spin echo images (**c**). (**a**): CT from PET/CT; (**b**) fused FDG-PET/CT; (**c**) T2 single shot fast spin echo; (**d**) fused FDG-PET/MRI; (**e**)ADC; (**f**) DWI

As illustrated in Fig. 21.3, the restricted diffusion evaluated on the DWI sequence assisted in the detection and characterization of a FDG-avid renal lesion that was missed on PET/CT due to being obscured by adjacent excreted activity in the renal collecting system [40].

Lymphoma patients undergo multiple contrast examination for staging and treatment monitoring; however, there is an increasing clinical concern over non-macrocyclic gadolinium-based agent deposition in the brain and body after serial examinations [74]; thus, careful review of contrast indication is highly

recommended. A recent publication [75] confirms the feasibility and high diagnostic accuracy of non-contrast FDG-PET/MRI and FDG-PET and that neither the application of contrast agents nor DWI leads to noticeable diagnostic improvement. Furthermore, the study concluded that PET/MRI is significantly superior to WB-MR-DWI for the evaluation of pediatric lymphoma. Agents such as ferumoxytol, an off-label MRI contrast agent, have been proposed as an alternative; however, there is limited pediatric data on its feasibility.

In summary, preliminary data demonstrate that PET/MRI is feasible in pediatric lymphoma patients and comparable to PET/CT for staging and treatment response assessment. Replacement of PET/CT with PET/MRI provides superior soft tissue contrast and functional MR imaging capabilities which can aid in lesion detection especially in solid organs, decreases exposure to ionizing radiation, and potentially limit the use of gadolinium-based contrast agents.

21.6 Brain Tumors

Primary brain tumors are the second most common tumor of childhood after leukemia and represent approximately 25% of childhood neoplasms [76]. Pediatric brain tumors are a diverse group of neoplasms with a wide range of biological aggressiveness and prognosis [77]. Key categories include astrocytomas and other tumors of glial origin, brain stem gliomas, CNS embryonal tumors including medulloblastoma, pineal tumors, CNS germ cell tumors, craniopharyngioma, ependymoma, and choroid plexus tumors. Treatment modalities for brain tumors include surgical resection, radiation therapy, and systemic therapies with cytotoxic, antiangiogenic, and immune-modulating agents. Depending on the tumor type and location, therapy often combines two or more of these modalities. A common treatment regimen is surgical resection followed by radiation therapy often in combination with chemotherapy. Over 70% of children with brain tumors will survive for over 5 years after diagnosis, but long-term disabilities are common due to both the tumor itself and the effects of treatment.

Brain MRI with contrast is the cornerstone of neuroimaging for pediatric neuro-oncology from the time of initial diagnosis through treatment planning and monitoring to long-term follow-up. Contrast-enhanced MRI has excellent sensitivity for detecting tumor with disrupted blood-brain barriers (BBB), while T2, FLAIR, and DWI sequences are valuable for evaluating non-enhancing lesions that do not have a grossly disrupted BBB. Despite its strengths, MRI has substantial limitations for defining tumor boundaries, guiding biopsy for non-enhancing lesions, and distinguishing treatment effects from recurrent tumor.

Combined PET/MRI is well suited to brain tumor imaging as the PET acquisition including dynamic studies for many PET tracers can be performed in the 45–60 min time required for a brain tumor MRI protocol. Data from adult patients suggest the kinetics of *O*-(2-[^{18}F]fluoroethyl)-L-tyrosine (FET) can distinguish high-grade from low-grade gliomas and can help distinguish radiation necrosis from recurrent tumor [78–82]. While dynamic PET is readily acquired on PET/CT systems, the dynamic acquisition occupies the PET/CT scanner much longer than a static brain or whole-body PET/CT study which can reduce patient throughput. The duration of dynamic PET studies with small-molecule PET tracers such as FDG and radiolabeled amino

acids is well matched to MRI for brain tumors. Unlike some other oncologic applications, CT plays a much smaller role in neuro-oncology compared to MRI and thus provides little beyond attenuation correction during PET/CT examinations.

Although FDG is effective for many solid tumors, it has substantial limitations in neuro-oncology. The high physiologic uptake of FDG in normal gray matter can obscure tumor tissue even when there is FDG uptake by tumor tissue. Additionally, posttreatment inflammation can lead to false-positive studies. Nevertheless, FDG does have some favorable properties for neuro-oncology. As in adults, higher FDG uptake is associated with more aggressive and higher-grade brain tumors in children [83, 84]. The most common pediatric brain tumors with high FDG uptake are glioblastoma and medulloblastoma, although some low-grade pilocytic astrocytomas can have high FDG uptake. There is significant overlap between many high- and low-grade tumors which can make assessment of tumor grade in an individual patient with FDG-PET alone challenging. FDG-PET has also been used to guide brain tumor biopsy based on the area of highest uptake [85, 86]. FDG-PET has been used to distinguish radiation necrosis from recurrent tumor when ambiguous contrast-enhancing lesions are present on MRI after radiation therapy. Recurrent high-grade gliomas typically have higher FDG uptake than radiation necrosis which has been proposed as a method for distinguishing these entities, although utility of FDG-PET for this application remains controversial [87–91]. An example of increased FDG uptake in a recurrent medulloblastoma is shown in Fig. 21.4.

Radiolabeled amino acids targeting system L amino acid transporters including 3,4,-dihydroxy6-[^{18}F]fluoro-L-phenylalanine (FDOPA), L-[^{11}C]methionine (MET), and FET are well-established PET tracers for brain tumor imaging. In 2016, this class of tracers was incorporated into the Response Assessment for Neuro-Oncology (RANO) recommendations for brain tumors [5]. System L transport is activated at the blood-brain barrier (BBB), allowing these tracers to reach the entire tumor volume. Additionally, higher levels of the system L family member, LAT1 (SLC7A5),

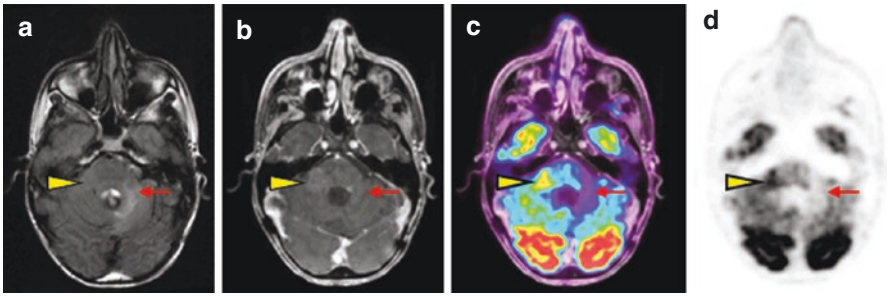

Fig. 21.4 FDG-PET/MRI in a 20-year-old male with suspected recurrence of medulloblastoma. A representative FLAIR image (**a**) demonstrates subtle signal hyperintensity in the region of the right cerebellar peduncle (*yellow arrow head*) and more conspicuous hyperintensity in the left cerebellar hemisphere (*red arrow*). There is contrast enhancement in the right middle cerebellar peduncle but not in the left cerebellar hemisphere (**b**). Fused FDG-PET/MRI (**c**) and PET only (**d**) images demonstrate increased FDG uptake in the right cerebellar peduncle lesion (*yellow arrow head*) but not the left cerebellar hemisphere lesion (*red arrow*), most consistent with recurrence and treatment effect in these locations, respectively. (**a**) FLAIR; (**b**) post-contrast T1; (**c**) fused FDG-PET/MRI; (**d**) FDG-PET

are associated with shorter overall survival in adult gliomas [92–94]. This class of PET tracers has been used extensively in adult neuro-oncology for surgical planning, monitoring response to chemotherapy, and detecting recurrent gliomas after completion of therapy [82, 95–99]. Although there are differences between FDOPA, MET, and FET, they have similar properties in terms of visualizing brain tumors and defining tumor margins [96, 100–102]. Compared to FDG, these tracers have relatively low uptake in the normal brain and less uptake by inflammatory lesions.

Limited studies in pediatric populations suggest that FET and other amino acids targeting system L transport have similar favorable diagnostic properties in pediatric patients as in adults [85, 103–106]. These data suggest that amino acid PET can guide stereotactic biopsy, distinguish high-grade from low-grade tumors, guide surgical resection, monitor response to systemic therapies, and distinguish treatment effects such as radiation necrosis from recurrent tumor. Larger studies are needed to define sensitivity, specificity, and diagnostic accuracy for these applications of amino acid PET in children. Examples of MET-PET/MRI to guide stereotactic biopsy and FDOPA-PET/MRI to monitor response to antiangiogenic therapy are shown in Figs. 21.5 and 21.6, respectively. Currently, very few studies have used amino acid PET combined with simultaneous PET/MRI in children with brain tumors [107, 108]. These studies demonstrate that simultaneous amino acid PET/MRI is feasible in pediatric neuro-oncology patients and that many older children can tolerate the 45 min PET/MRI studies without sedation or anesthesia.

21.7 Sarcoma

Pediatric sarcomas are a heterogeneous group of tumors accounting for approximately 10% of childhood solid tumors, where the various subtypes have distinct biological patterns and incidence (National Cancer Institute. Homepage on the Internet. Available at: http://www.cancer.gov. Accessed February 1, 2016). Sarcomas are divided into two main groups: bone sarcoma (BS) and soft tissue sarcomas (STS). The most common bone sarcomas are osteosarcoma (OS) and Ewing sarcoma (ES); both tumors have a peak incidence during adolescence with the presence of metastases at diagnosis being one of the strongest predictors of survival [109]. The soft tissue sarcomas are further subdivided into rhabdomyosarcomas (RMS), the most common soft tissue malignancy in children and adolescent, and non-rhabdomyosarcomas (N-RMS) which are mainly seen in adolescents. The two most common histologic RMS variants encountered in the pediatric population are embryonal rhabdomyosarcomas (ERMS) which occur in about 65–75% of patients and alveolar rhabdomyosarcoma (ARMS) subtypes.

Treatment of primary musculoskeletal malignancies requires systemic multi-agent therapy, including systemic chemotherapy and local control of tumors. Local-regional control may be achieved with surgery and/or radiation therapy and neoadjuvant chemotherapy. Lesions inadequately treated locally are associated with poor outcome and treatment failure. The 3–5-year event-free survival rates for patients with localized sarcomas are 60–70% [110], for patients with metastatic disease below 20–30%, and for patients with relapsed disease less than 10–20% [111–113].

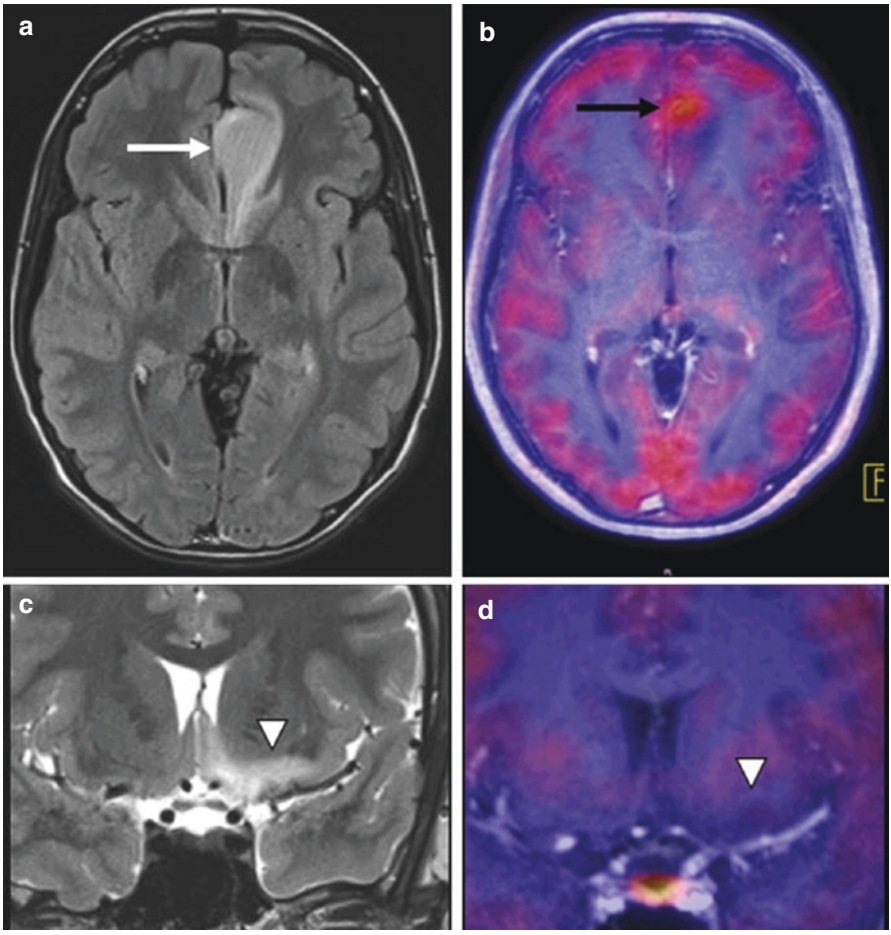

Fig. 21.5 MET-PET/MR imaging in a 15-year-old boy with a non-enhancing multifocal primary brain tumor. The FLAIR MR image (**a**) shows signal hyperintensity in the left frontal lobe adjacent to the falx (*white arrow*). The T2-weighted MR image (**c**) shows signal hyperintensity more inferiorly in the left from lobe (*arrow head*). The fused MET-PET/MR images show focal uptake in the left frontal lesion along the falx (**b**, *black arrow*) but not in the more inferior left frontal lobe (**d**). This focus of increase MET uptake was used to guide stereotactic biopsy and yielded anaplastic astrocytoma. *This figure is courtesy of Drs. Franz Wolfgang Hirsch and Regine Kluge from the University Hospital of Leipzig, Germany*. (**a**) FLAIR; (**b**) fused MET-PET/MRI post-contrast T1; (**c**) T2; (**d**) fused MET-PET/MRI post-contrast T1

The frequency of distant metastasis in pediatric sarcomas varies from 10 to 12% [60]. Regional lymph node disease is a component of the risk-based treatment stratification for rhabdomyosarcoma, and it has been noted that regional lymph node involvement affects the prognosis in patients with alveolar RMS, while outcomes in patients with nodal involvement (N1) are more similar to distant metastatic disease rather than local disease [114].

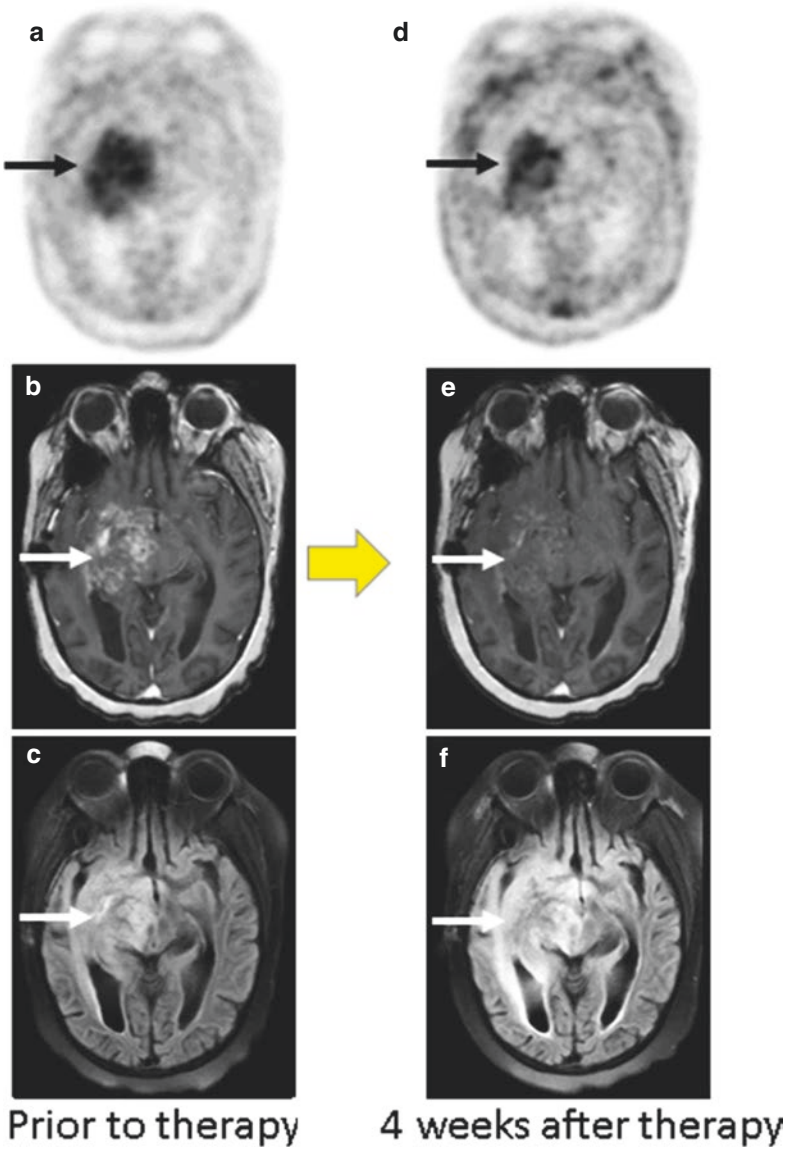

Fig. 21.6 FDOPA-PET/MR imaging in an 8-year-old girl with small cell glioma before and after bevacizumab therapy. The initial FDOPA-PET image (**a**) demonstrates increased uptake throughout the mass (*arrow*) involving the right frontal and temporal lobe as well as the brainstem. This mass shows heterogeneous enhancement on the post-contrast MR image (**b**) and FLAIR signal hyperintensity (**c**). After 4 weeks of bevacizumab, the uptake of FDOPA decreased slightly but there is persistent activity (**d**). The contrast enhancement has nearly completely resolved (**e**), but the FLAIR signal abnormality is unchanged (**f**). The persistent FDOPA uptake suggests poor response to therapy, and the patient subsequently had progressive disease. This case was part of a recent publication examining the potential of FDOPA-PET/MRI to predict response to bevacizumab early in the course of therapy [108]. (**a**) pre-bevacizumab FDOPA-PET; (**b**) pre-bevacizumab post-contrast T1; (**c**) pre-bevacizumab FLAIR; (**d**) post-bevacizumab FDOPA-PET; (**e**) post-bevacizumab post-contrast T1; (**f**) post-bevacizumab FLAIR

Although musculoskeletal sarcomas may have distinguishing imaging features on radiograph or CT, MRI is the preferred modality for assessment of the primary tumor size and extent of organ involvement due to its superior soft tissue contrast [115]. However, the role of MRI is limited in assessment of treatment response and follow-up [116] due to tumor changes during the regression phase, accounting for necrosis, hemorrhage, proliferation of granulation tissue, fibrosis, and organization of a pseudo-capsule [117]. As a result, an increase in tumor volume may be observed in responders, and MRI imaging alone is insufficient to distinguish residual viable tumor from granulation tissue given that both are highly vascular and demonstrate contrast enhancement. In addition, the length of intramedullary signal abnormalities does not vary in response to chemotherapy, which results in uncertainties in the evaluation of posttreatment tumor volume response.

Approximately 20–25% of patients with bone sarcomas present with radiographically detectable distant metastases [118] with the most common site of involvement being the lungs. The primary imaging modality for evaluation of pulmonary involvement is the CT. In patients with RMS, the most common sites for metastases are the lungs, bones, and bone marrow. Given the limitation of MRI for the detection of small lung metastasis, the addition of high-resolution CT of the thorax is generally recommended in the staging of pediatric sarcoma patients. Since RMS can arise throughout the body, metastatic sites may be located outside the field of view; thus, whole-body MRI may be a helpful imaging modality for staging, although there are limited publications with respect to the pediatric population [119, 120].

Currently, whole-body FDG-PET/CT is not considered a standard examination for evaluating disease extent in sarcoma patients [121], despite the promising results from a small number of studies which found FDG-PET/CT better in identifying occult non-pulmonary metastasis compared to conventional imaging [122–125]. The study by Quartuccio et al. [126], which evaluated the diagnostic performance of FDG-PET versus conventional imaging for bone sarcoma in 64 pediatric patients (osteosarcoma 20/64 and Ewing sarcoma 44/64) at initial staging and follow-up, showed that both FDG-PET/CT and MRI were more accurate than CT and skeletal scintigraphy with [^{99m}Tc]MDP in the follow-up. In addition, the authors noted that FDG-PET/CT provided greater diagnostic benefit for ES during clinical management than for OS. In several studies, reduction in the standardized uptake value (SUV) and the absolute post-therapeutic SUV was found to significantly discriminate responders from nonresponders in pediatric osteosarcoma patients [127], but tumor volume reduction measured by MR or CT did not significantly discriminate responders from nonresponders in either subgroup.

The intensity of FDG uptake in the primary and recurrent tumor may provide additional diagnostic and prognostic information with high-grade tumors tending toward higher FDG avidity than low-grade tumors due to higher cellularity, although no established definitive SUV cutoff has been identified. Thus, the identification of areas with high FDG metabolic activity for open biopsies may potentially identify the most aggressive pathology, which may affect treatment planning and prognosis. In addition, several studies have showed significantly prolonged event-free and overall survival for osteosarcomas patients with low FDG uptake at baseline [128] with similar results for RMS.

In a pediatric oncology study using an integrated PET/MR scanner following chemotherapy, Hirsch et al. [71] showed that metabolic changes take place earlier than the morphological response. Similar results were reported on the FDG-PET/MRI study [129] for staging and restaging in pediatric rhabdomyosarcoma (n = 15/270), soft tissue sarcoma, and bone sarcoma (n = 21/270) which concluded that combined PET/MRI was the methodology of choice for accurate tumor staging. In patients with OS who were imaged with sequential FDG-PET/CT and MRI, early changes in FDG SUV or MTV were noted with corresponding changes on MRI, after one cycle of neoadjuvant chemotherapy.

In pediatric sarcomas, FDG-PET/MRI has potential roles for initial staging as illustrated in Fig. 21.7 and for evaluating tumor response during and after therapy. MRI imaging alone is limited in its ability to accurately distinguish between post-treatment changes from tumor recurrence, due to persistent morphological tissue changes. The combined metabolic imaging capabilities of PET with the superb soft tissue contrast of MRI provide relevant information on regions with complex anatomy such as the neck and pelvis, as shown in Fig. 21.8. In addition, better soft tissue resolution allows for more accurate differentiation from physiologic uptake of) ormal organs, such as ovaries, from uptake associated with malignancy, as illustrated in Fig. 21.9. In this patient, the correct diagnosis was physiologic activity in the ovaries and not bilateral FDG-avid external iliac lymphadenopathy. This diagnosis lead

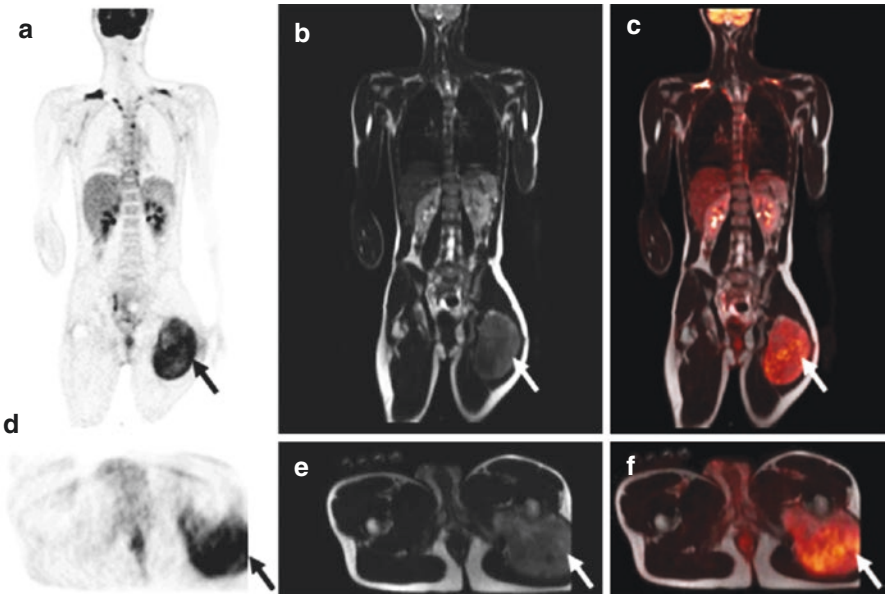

Fig. 21.7 17-year-old boy with spindle cell rhabdomyosarcoma undergoing simultaneous FDG-PET/MRI for initial staging. FDG-avid soft tissue mass is seen extending into the posterior adductor compartments of the left thigh (**a**–**c**) without locoregional or distant metastasis disease. Dedicated regional PET/MRI (**d**–**f**) demonstrates avid mass with no bone marrow infiltration. (**a**, **d**) FDG-PET; (**b**, **e**) T2 single shot fast spin echo; (**c**, **f**) fused FDG-PET/MRI

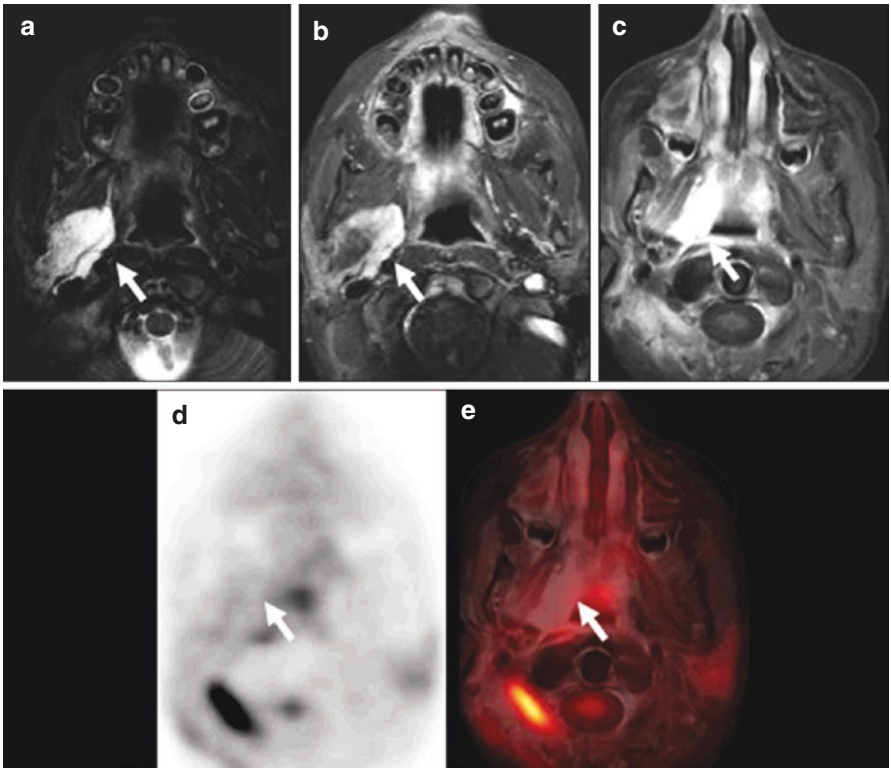

Fig. 21.8 FDG-PET/MRI performed in an 8-year-old girl with right parameningeal rhabdomyosarcoma before and after therapy. Neck MRI at initial presentation (**a**, **b**) and simultaneous FDG PET/MRI (**c**–**e**) after treatment demonstrates T2 hyperintense enhancing right parapharyngeal mass (*white arrows*). PET/MRI showed persistent increased enhancing soft tissue in the right parapharyngeal resection bed (**c**) after resection and chemoradiation with no FDG uptake on PET (**e**), favored to represent non-viable tumor. Neck MRI (**a**) T2-weighted image; (**b**) T1-weighted image with contrast, PET/MRI; (**c**) T1-weighted images with contrast; (**d**) FDG PET; (**e**) Fused T1-weighted image with FDG PET

to a change in patient management by reducing the radiation field to exclude the pelvis and thus decreasing potential secondary treatment side effects, including premature fusion of the growth plates resulting in asymmetry of muscles and bones in the treated area and infertility. For evaluation of pulmonary metastasis, a non-contrast chest CT performed before or after the PET/MRI should be included in the protocol. The role of PET/MRI for pediatric sarcomas is evolving, and more studies will be needed to document outcomes and impact on clinical patient management.

In summary, pediatric patients being assessed for bone or soft tissues tumors routinely require both PET and MR imaging. These patients are well suited for a simultaneous PET/MRI examination combining MRI for locoregional tumor staging and FDG-PET for nodal and distant metastatic staging. PET/MRI superior soft tissue contrast, anatomic resolution, and functional MR techniques combined with PET metabolic imaging improve the characterization of lesions and allow for early response assessment in patients undergoing therapy.

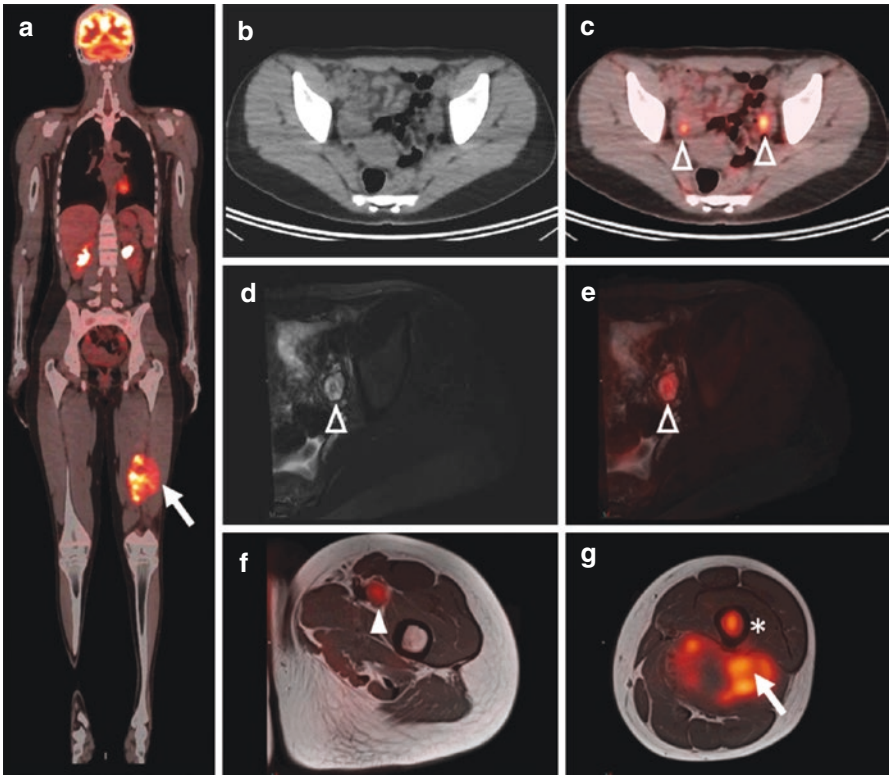

Fig. 21.9 FDG-PET/MRI performed in a 14-year-old girl with extra-osseous Ewing's sarcoma. Whole body FDG-PET/CT demonstrates FDG-avid left posterior thigh mass (**a**, *white arrow*) and bilateral foci of FDG-uptake in the pelvis (**c**, *arrowhead*), which was wrongly diagnosed as bilateral external iliac lymphadenopathy on PET/CT. MRI of the pelvis and left lower extremity demonstrates normal ovary (**d** and **e**, *open arrow head*) which corresponded to the focus of increased uptake on FDG-PET/CT. Fused sequential FDG PET and MRI show a left femoral FDG-avid regional lymph node (**f**, *white arrow head*) and the hypermetabolic extra-osseous mass (**g**, *white arrow*) with bone marrow infiltration (**g**, *asterisk*). (**a**) whole body FDG-PET/CT; (**b**) CT of FDG-PET/CT; (**c**) Fused FDG-PET/CT; (**d**) T2 weighted images; (**e**–**g**) fused FDG-PET with T2 and T1-weighted images (**f**, **g**)

21.8 Neuroblastoma

Neuroblastoma (NB) is the third most common childhood cancer and represents 6% of the total cases of pediatric malignancies (ages 0–14 years) [76] and is the most frequent extracranial solid tumor affecting children. The median age of diagnosis is 19 months, with 90% of the cases diagnosed in children younger than 5 years. It is rare in adolescents and adults [130]. Neuroblastoma is an embryonic tumor derived from neuroectodermal cells of the neural crest of the sympathetic nervous system. It may develop anywhere in the sympathetic nervous system, and approximately 50% of cases originate in the adrenal medulla, 30% in the paraspinal sympathetic ganglia in the abdomen, 6–7% in the neck, 15% in the chest, and 2–3% in the pelvis, respectively [131]. The variable histological, epidemiological, and biological characteristics of

neuroblastoma tumors can produce changes from spontaneous regression to maturation to more aggressive grade [132, 133]. Metastasis in neuroblastoma patients is noted in 60–70% of the cases at diagnosis [134, 135]. The most frequent metastatic sites are the bone marrow, bone and lymph nodes and to a lesser extent the liver and skin. Central nervous system and pulmonary metastases are less common, affecting more frequently adolescents, and associated with poor outcomes [136].

The treatment and outcome of neuroblastoma are strongly dependent on the patient's age, risk assessment, and disease stage. There are effective therapies for children or under 12 months of age diagnosed with low- to intermediate-risk disease, with excellent survival rates. The survival rates are much less favorable in children over the age of 12 months who present with advanced-stage disease despite the availability of multimodality therapies [133, 137]. Overall, surgical resection is the preferred treatment of localized tumors, where extensive disease requires combined therapy. Thus, accurate staging and risk stratification play an important role in patient management and prognosis.

The current diagnostic imaging examinations to stage neuroblastoma include ultrasonography (US), MRI and/or CT, and [^{123}I]MIBG planar and SPECT scintigraphy that targets the norepinephrine transporter in neuroblastoma cells. Whole-body MRI for neuroblastoma has demonstrated utility in detecting distant metastasis and bone marrow involvement [138, 139]. The major limitation of morphological imaging, including MRI, is the accurate detection of nodal metastases and assessment of tumor viability in the posttreatment setting [140]. FDG-PET and other PET tracers do not currently play a substantial role in the routine evaluation of neuroblastoma patients at most centers. Promising PET tracers for neuroblastoma include [^{124}I]MIBG, ^{68}Ga-labeled somatostatin receptor ligands, and the ^{18}F-labeled amino acid FDOPA [7, 20, 141–143].

[^{123}I]MIBG is a SPECT tracer that has been part of the standard of care for whole-body staging of neuroblastoma patients, with sensitivities over 85% and specificities over 90% [144], particularly for bone and bone marrow diseases. [^{123}I]MIBG plays a critical role in the evaluation of treatment response since MIBG uptake is seen in 90–95% of the patients with neuroblastoma [145]. MIBG imaging is overall considered more specific and superior to FDG-PET, particularly in the delineation of residual disease although [^{123}I]MIBG scintigraphy may produce false-negative results in 10–20% of cases [146, 147]. [^{124}I]MIBG could be used for PET/CT and PET/MRI, but this tracer is not currently widely available.

Currently, the role of FDG-PET is limited, although neuroblastoma demonstrates FDG uptake; its function is providing complementary diagnostic information to assess MIBG-negative tumors with positive clinical symptoms or morphological images [148, 149]. Limitations in staging neuroblastoma with FDG-PET include uptake not related to catecholamine metabolism; low sensitivity to identify bone or bone marrow involvement, which is a common site of disease; and marked changes in FDG uptake in patients receiving chemotherapy or granulocyte colony-stimulating factor (G-CSF) [147, 150].

Several publications have shown in vitro using autoradiography and immunohistochemistry the expression of somatostatin receptor in up to 77–89% in neuroblastoma cells [151, 152]. SSTRs can be targeted with ^{68}Ga-labeled peptides for PET imaging. Recent pediatric study using [^{68}Ga]DOTATE-PET/CT showed

additional sites of disease in up to 38% pediatric patients compared with MIBG [153]. A limited number of studies evaluating the use of PET for somatostatin receptor imaging in pediatric neuroblastoma selected for peptide receptor radionuclide therapy (PRRT) have been published. Preliminary results have shown that a high proportion of neuroblastoma patients (75%, 6/8 patients) have sufficient somatostatin receptor expression on their tumors to be considered for PRRT, especially in children who have failed prior treatment with chemotherapy and [^{131}I] MIBG radionuclide therapy [154].

The radiolabeled amino acid FDOPA is also a promising PET tracer for imaging neuroblastoma. Small studies with FDOPA-PET in this patient population have reported high sensitivity and specificity of 97.6% and 87.5% [155] and sensitivity and accuracy of 95 and 96% [142] which are significantly higher than that of [^{123}I] MIBG scintigraphy. Comparison of FDOPA-PET/CT with CT and MR demonstrated in a prospective study on 21 patients with advanced-stage neuroblastoma (III–IV) that FDOPA-PET/CT had significantly higher sensitivity, specificity, and accuracy compared to MRI and CT with higher lesion detection than CT/MRI in the bone, bone marrow, lymph node, and soft tissue recurrences [141]. An example of FDOPA-PET/MRI in neuroblastoma is shown in Fig. 21.10.

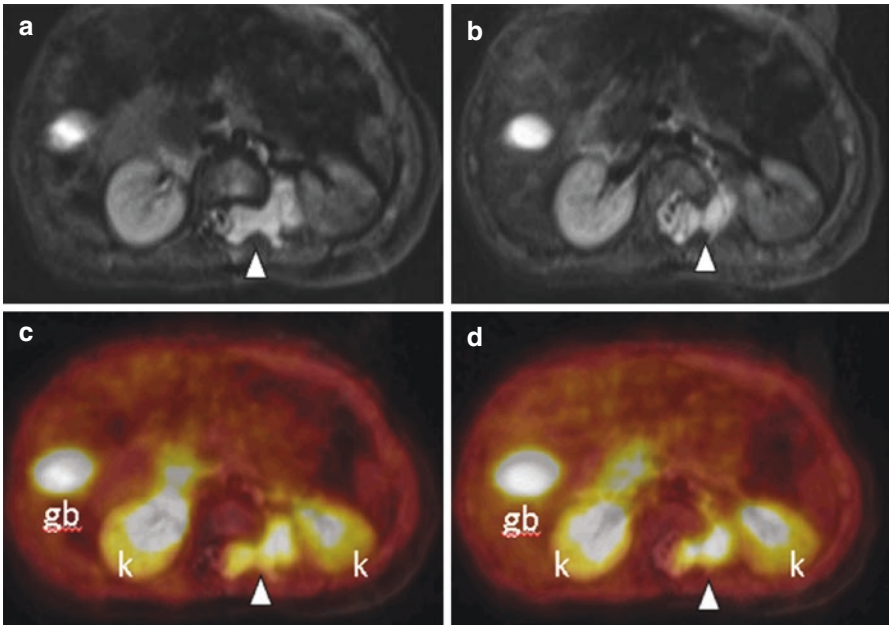

Fig. 21.10 FDOPA-PET/MRI performed in a 2-year old boy undergoing initial staging for a neuroblastoma. The T2 fat saturated MR images (**a**, **b**) show a lobulated T2 hyperintense mass involving the central spinal canal, a spinal neuroforamen and the left paraspinal region (*arrow head*) representing the primary tumor. This lesion demonstrates increased uptake of FDOPA on the fused PET/MRI images (**c**, **d**). No metastases were identified. Note the normal excreted activity in the kidneys (*k*) and gallbladder (*gb*). *This figure is courtesy of Drs. Franz Wolfgang Hirsch and Regine Kluge from the University Hospital of Leipzig, Germany*. (**a**, **b**) T2 fat sat; (**c**, **d**) fused FDOPA-PET/MRI

Pediatric PET/MRI publications of mixed cancer populations, including small sample size of patients with neuroblastoma, demonstrated that FDG-PET/MRI is equivalent to FDG-PET/CT for oncologic imaging in young children for the assessment of tumor spread and monitoring of therapeutic courses [22, 71]. Furthermore, MRI can provide additional diagnostic imaging information on lesions with inconclusive FDG uptake on PET, such as homogeneous bone marrow FDG uptake without visible findings on CT in patients with bone marrow infiltration [23]. In this context, additional MRI functional information can be implemented in standard PET/MRI protocols, such as DWI to identify bone marrow infiltration thus providing a complementary diagnostic tool.

In summary, there are a range of PET/MRI tracers including FDG, ^{68}Ga-labeled somatostatin receptor ligands, FDOPA, and [^{124}I]MIBG that have great potential for imaging neuroblastoma. However, there is limited experience with these tracers in pediatric neuroblastoma with PET/CT, and only a few publications report their use with PET/MRI. The increasing availability of [^{68}Ga]DOTATATE and similar agents coupled with the potential for PRRT targeting somatostatin receptors could help enable the near-term growth of PET/MRI for neuroblastoma.

21.9 Conclusions and Future Directions

PET/MRI is clearly a promising hybrid modality for applications in pediatric oncology through reducing exposure to ionizing radiation and providing a single examination that combines metabolic, anatomic, and functional imaging. As in adults, children that require whole-body PET for staging as well as dedicated organ/regional MRI for tumor staging may benefit from simultaneous PET/MRI. The acquisition of both PET and MRI in the same session reduces the number of sedation/aesthesia and decreases misregistration caused by patient motion or physiologic changes. However, there is a need to produce high-quality evidence to demonstrate that combined PET/MRI examinations are superior to separately acquired PET/CT and MRI studies for specific indications in pediatric oncology.

Several factors are likely to determine the level of utilization of PET/MRI for pediatric oncology. First, a major current limitation for PET/MRI for adults and children is the cost of these systems and the relatively small number of imaging and referring physicians familiar with this technology. More universal availability will require adequate reimbursement, decreased cost differential between PET/MRI and PET/CT systems, and incorporation of PET/MRI into physician and technologist training. Second, the availability and reimbursement of new PET tracers for routine clinical use will be key factors for expanding the growth of both PET/CT and PET/MRI. Strong data showing diagnostic efficacy that leads to patient management and incorporation of PET tracers and PET/MRI in nationally and internationally recognized cancer management guidelines are needed. The studies needed to generate this type of data can be challenging in pediatric oncology due to the relatively small number of pediatric cancer patients combined with the limited number of sites with PET/MRI. Finally, the most common type of pediatric malignancy is leukemia,

which typically does not include PET as part of its routine diagnostic workup. The availability of PET tracers that can detect early response to therapy beyond what is possible by blood tests and marrow biopsies would be a major advance in PET for pediatric leukemia patients. Pediatric PET/MRI is expanding and remains an active area of clinical research with the expectation that progress on many of these fronts will continue.

References

1. Smith TA. The rate-limiting step for tumor [^{18}F]fluoro-2-deoxy-D-glucose (FDG) incorporation. Nucl Med Biol. 2001;28:1–4.
2. Ganapathy V, Thangaraju M, Prasad PD. Nutrient transporters in cancer: relevance to Warburg hypothesis and beyond. Pharmacol Ther. 2009;121:29–40.
3. Potter M, Newport E, Morten KJ. The Warburg effect: 80 years on. Biochem Soc Trans. 2016;44:1499–505.
4. Huang C, McConathy J. Radiolabeled amino acids for oncologic imaging. J Nucl Med. 2013;54:1007–10.
5. Albert NL, Weller M, Suchorska B, et al. Response assessment in neuro-oncology working group and European Association for Neuro-Oncology recommendations for the clinical use of PET imaging in gliomas. Neuro-Oncology. 2016;18:1199.
6. Dunkl V, Cleff C, Stoffels G, et al. The usefulness of dynamic O-(2-^{18}F-fluoroethyl)-L-tyrosine PET in the clinical evaluation of brain tumors in children and adolescents. J Nucl Med. 2015;56:88–92.
7. Kroiss A, Putzer D, Uprimny C, et al. Functional imaging in pheochromocytoma and neuroblastoma with ^{68}Ga-DOTA-Tyr 3-octreotide positron emission tomography and ^{123}I-metaiodobenzylguanidine. Eur J Nucl Med Mol Imaging. 2011;38:865–73.
8. Hope TA, Pampaloni MH, Nakakura E, et al. Simultaneous ^{68}Ga-DOTA-TOC PET/MRI with gadoxetate disodium in patients with neuroendocrine tumor. Abdom Imaging. 2015;40:1432–40.
9. Kunz WG, Jungblut LM, Kazmierczak PM, et al. Improved detection of transosseous meningiomas using ^{68}Ga-DOTATATE PET-CT compared to contrast-enhanced MRI. J Nucl Med. 2017;58(10):1580–87. https://doi.org/10.2967/jnumed.117.191932. Epub 2017 Apr 27
10. Afshar-Oromieh A, Giesel FL, Linhart HG, et al. Detection of cranial meningiomas: comparison of ^{68}Ga-DOTATOC PET/CT and contrast-enhanced MRI. Eur J Nucl Med Mol Imaging. 2012;39:1409–15.
11. Kwekkeboom DJ, Kam BL, van Essen M, et al. Somatostatin-receptor-based imaging and therapy of gastroenteropancreatic neuroendocrine tumors. Endocr Relat Cancer. 2010;17:R53–73.
12. Strosberg J, El-Haddad G, Wolin E, et al. Phase 3 trial of ^{177}Lu-Dotatate for Midgut neuroendocrine tumors. N Engl J Med. 2017;376:125–35.
13. Archier A, Varoquaux A, Garrigue P, et al. Prospective comparison of ^{68}Ga-DOTATATE and ^{18}F-FDOPA PET/CT in patients with various pheochromocytomas and paragangliomas with emphasis on sporadic cases. Eur J Nucl Med Mol Imaging. 2016;43:1248–57.
14. Barthlen W, Blankenstein O, Mau H, et al. Evaluation of [^{18}F]fluoro-L-DOPA positron emission tomography-computed tomography for surgery in focal congenital hyperinsulinism. J Clin Endocrinol Metab. 2008;93:869–75.
15. Liu YL, Lu MY, Chang HH, et al. Diagnostic FDG and FDOPA positron emission tomography scans distinguish the genomic type and treatment outcome of neuroblastoma. Oncotarget. 2016;7:18774–86.
16. Barthlen W, Varol E, Empting S, et al. Surgery in focal congenital hyperinsulinism (CHI) - the "hyperinsulinism Germany international" experience in 30 children. Pediatr Endocrinol Rev. 2016;14:129–37.

17. Dercle L, Deandreis D, Terroir M, Leboulleux S, Lumbroso J, Schlumberger M. Evaluation of ^{124}I PET/CT and ^{124}I PET/MRI in the management of patients with differentiated thyroid cancer. Eur J Nucl Med Mol Imaging. 2016;43:1006–10.
18. Vrachimis A, Weckesser M, Schafers M, Stegger L. Imaging of differentiated thyroid carcinoma: ^{124}I-PET/MRI may not be superior to ^{124}I-PET/CT. Eur J Nucl Med Mol Imaging. 2016;43:1183–4.
19. Binse I, Poeppel TD, Ruhlmann M, et al. Imaging with ^{124}I in differentiated thyroid carcinoma: is PET/MRI superior to PET/CT? Eur J Nucl Med Mol Imaging. 2016;43:1011–7.
20. Cistaro A, Quartuccio N, Caobelli F, et al. ^{124}I-MIBG: a new promising positron-emitting radiopharmaceutical for the evaluation of neuroblastoma. Nucl Med Rev Cent East Eur. 2015;18:102–6.
21. Hartung-Knemeyer V, Rosenbaum-Krumme S, Buchbender C, et al. Malignant pheochromocytoma imaging with [^{124}I]mIBG PET/MR. J Clin Endocrinol Metab. 2012;97:3833–4.
22. Gatidis S, Schmidt H, Gucke B, et al. Comprehensive oncologic imaging in infants and preschool children with substantially reduced radiation exposure using combined simultaneous ^{18}F-Fluorodeoxyglucose positron emission tomography/magnetic resonance imaging: a direct comparison to ^{18}F-Fluorodeoxyglucose positron emission tomography/computed tomography. Investig Radiol. 2016;51:7–14.
23. Schafer JF, Gatidis S, Schmidt H, et al. Simultaneous whole-body PET/MR imaging in comparison to PET/CT in pediatric oncology: initial results. Radiology. 2014;273:220–31.
24. Drzezga A, Souvatzoglou M, Eiber M, et al. First clinical experience with integrated whole-body PET/MR: comparison to PET/CT in patients with oncologic diagnoses. J Nucl Med. 2012;53:845.
25. Tian J, Fu L, Yin D, et al. Does the novel integrated PET/MRI offer the same diagnostic performance as PET/CT for oncological indications? PLoS One. 2014;9:e90844.
26. Heusch P, Buchbender C, Beiderwellen K, et al. Standardized uptake values for [^{18}F] FDG in normal organ tissues: comparison of whole-body PET/CT and PET/MRI. Eur J Radiol. 2013;82:870.
27. Spick C, Herrmann K, Czernin J. ^{18}F-FDG PET/CT and PET/MRI perform equally well in cancer: evidence from studies on more than 2,300 patients. J Nucl Med. 2016;57:420–30.
28. Eiber M, Martinez-Moller A, Souvatzoglou M, et al. Value of a Dixon-based MR/PET attenuation correction sequence for the localization and evaluation of PET-positive lesions. Eur J Nucl Med Mol Imaging. 2011;38:1691–701.
29. Rascon J, Rageliene L, Stankeviciene S, et al. An assessment of iron overload in children treated for cancer and nonmalignant hematologic disorders. Eur J Pediatr. 2014;173:1137–46.
30. Taouli B, Koh DM. Diffusion-weighted MR imaging of the liver. Radiology. 2010;254:47–66.
31. Mohd Zaki F, Moineddin R, Grant R, Chavhan GB. Accuracy of pre-contrast imaging in abdominal magnetic resonance imaging of pediatric oncology patients. Pediatr Radiol. 2016;46:1684–93.
32. Murata N, Gonzalez-Cuyar LF, Murata K, et al. Macrocyclic and other non-group 1 gadolinium contrast agents deposit low levels of gadolinium in brain and bone tissue: preliminary results from 9 patients with normal renal function. Investig Radiol. 2016;51:447–53.
33. Murata N, Murata K, Gonzalez-Cuyar LF, Maravilla KR. Gadolinium tissue deposition in brain and bone. Magn Reson Imaging. 2016;34:1359–65.
34. Klenk C, Gawande R, Uslu L, et al. Ionising radiation-free whole-body MRI versus ^{18}F-fluorodeoxyglucose PET/CT scans for children and young adults with cancer: a prospective, non-randomised, single-centre study. Lancet Oncol. 2014;15:275–85.
35. Sawicki LM, Grueneisen J, Buchbender C, et al. Evaluation of the outcome of lung nodules missed on ^{18}F-FDG PET/MRI compared with ^{18}F-FDG PET/CT in patients with known malignancies. J Nucl Med. 2016;57:15–20.
36. Raad RA, Friedman KP, Heacock L, Ponzo F, Melsaether A, Chandarana H. Outcome of small lung nodules missed on hybrid PET/MRI in patients with primary malignancy. J Magn Reson Imaging. 2016;43:504–11.
37. Lee KH, Park CM, Lee SM, et al. Pulmonary nodule detection in patients with a primary malignancy using hybrid PET/MRI: is there value in adding contrast-enhanced MR imaging? PLoS One. 2015;10:e0129660.

38. Burris NS, Johnson KM, Larson PE, et al. Detection of small pulmonary nodules with ultrashort echo time sequences in oncology patients by using a PET/MR system. Radiology. 2016;278:239–46.
39. National Research Council (U.S.) Committee to assess health risks from exposure to low level of ionizing radiation. In: Health risks from exposure to low levels of ionizing radiation: BEIR VII phase, vol. 2. Washington, DC: National Academies Press; 2006.
40. Ponisio MR, McConathy J, Laforest R, Khanna G. Evaluation of diagnostic performance of whole-body simultaneous PET/MRI in pediatric lymphoma. Pediatr Radiol. 2016;46:1258–68.
41. Sher AC, Seghers V, Paldino MJ, et al. Assessment of sequential PET/MRI in comparison with PET/CT of pediatric lymphoma: a prospective study. Am J Roentgenol. 2016;206:623–31.
42. Harrison JD, Streffer C. The ICRP protection quantities, equivalent and effective dose: their basis and application. Radiat Prot Dosim. 2007;127:12–8.
43. Valentin J. The 2007 recommendations of the international commission on radiological protection. ICRP publication 103. Ann ICRP. 2007;37:1–332.
44. ICRP. Radiation dose to patients from radiopharmaceuticals. Addendum 3 to ICRP publication 53. ICRP publication 106. Approved by the Commission in October 2007. Ann ICRP. 2008;38:1–197.
45. Raman SP, Mahesh M, Blasko RV, Fishman EK. CT scan parameters and radiation dose: practical advice for radiologists. J Am Coll Radiol. 2013;10:840–6.
46. Miglioretti DL, Johnson E, Williams A, et al. The use of computed tomography in pediatrics and the associated radiation exposure and estimated cancer risk. JAMA Pediatr. 2013;167:700–7.
47. Seith F, Schmidt H, Kunz J, et al. Simulation of tracer dose reduction in ^{18}F FDG PET/MRI: Effects on oncologic reading, image quality and artifacts. J Nucl Med. 2017;58(10):1699–1705.
48. Gatidis S, Schmidt H, la Fougere C, Nikolaou K, Schwenzer NF, Schafer JF. Defining optimal tracer activities in pediatric oncologic whole-body ^{18}F-FDG-PET/MRI. Eur J Nucl Med Mol Imaging. 2016;43:2283–9.
49. Minamimoto R, Levin C, Jamali M, et al. Improvements in PET image quality in time of flight (TOF) simultaneous PET/MRI. Mol Imaging Biol. 2016;18:776–81.
50. Kaatsch P. Epidemiology of childhood cancer. Cancer Treat Rev. 2010;36:277–85.
51. Friedman DL, Chen L, Wolden S, et al. Dose-intensive response-based chemotherapy and radiation therapy for children and adolescents with newly diagnosed intermediate-risk Hodgkin lymphoma: a report from the Children's oncology group study AHOD0031. J Clin Oncol. 2014;32:3651–8.
52. Mauz-Korholz C, Metzger ML, Kelly KM, et al. Pediatric Hodgkin lymphoma. J Clin Oncol. 2015;33:2975–85.
53. Burkhardt B, Zimmermann M, Oschlies I, et al. The impact of age and gender on biology, clinical features and treatment outcome of non-Hodgkin lymphoma in childhood and adolescence. Br J Haematol. 2005;131:39–49.
54. Bhatia S, Yasui Y, Robison LL, et al. High risk of subsequent neoplasms continues with extended follow-up of childhood Hodgkin's disease: report from the late effects study group. J Clin Oncol. 2003;21:4386–94.
55. Constine LS, Tarbell N, Hudson MM, et al. Subsequent malignancies in children treated for Hodgkin's disease: associations with gender and radiation dose. Int J Radiat Oncol Biol Phys. 2008;72:24–33.
56. Dores GM, Metayer C, Curtis RE, et al. Second malignant neoplasms among long-term survivors of Hodgkin's disease: a population-based evaluation over 25 years. J Clin Oncol. 2002;20:3484–94.
57. Bhakta N, Liu Q, Yeo F, et al. Cumulative burden of cardiovascular morbidity in paediatric, adolescent, and young adult survivors of Hodgkin's lymphoma: an analysis from the St Jude lifetime cohort study. Lancet Oncol. 2016;17:1325–34.
58. Littooij AS, Kwee TC, Enriquez G, et al. Whole-body MRI reveals high incidence of osteonecrosis in children treated for Hodgkin lymphoma. Br J Haematol. 2017;176:637–42.
59. Guimaraes MD, Noschang J, Teixeira SR, et al. Whole-body MRI in pediatric patients with cancer. Cancer Imaging. 2017;17:6.

60. Siegel MJ, Acharyya S, Hoffer FA, et al. Whole-body MR imaging for staging of malignant tumors in pediatric patients: results of the American College of Radiology Imaging Network 6660 trial. Radiology. 2013;266:599–609.
61. Kwee TC, Takahara T, Ochiai R, et al. Complementary roles of whole-body diffusion-weighted MRI and ^{18}F-FDG PET: the state of the art and potential applications. J Nucl Med. 2010;51:1549–58.
62. Kwee TC, Takahara T, Luijten PR, Nievelstein RA. ADC measurements of lymph nodes: inter- and intra-observer reproducibility study and an overview of the literature. Eur J Radiol. 2010;75:215–20.
63. Herrmann K, Queiroz M, Huellner MW, et al. Diagnostic performance of FDG-PET/MRI and WB-DW-MRI in the evaluation of lymphoma: a prospective comparison to standard FDG-PET/CT. BMC Cancer. 2015;15:1002.
64. Weiler-Sagie M, Bushelev O, Epelbaum R, et al. ^{18}F-FDG avidity in lymphoma readdressed: a study of 766 patients. J Nucl Med. 2010;51:25–30.
65. Montravers F, McNamara D, Landman-Parker J, et al. [^{18}F]FDG in childhood lymphoma: clinical utility and impact on management. Eur J Nucl Med Mol Imaging. 2002;29:1155–65.
66. Hermann S, Wormanns D, Pixberg M, et al. Staging in childhood lymphoma: differences between FDG-PET and CT. Nuklearmedizin. 2005;44:1–7.
67. London K, Cross S, Onikul E, Dalla-Pozza L, Howman-Giles R. ^{18}F-FDG PET/CT in paediatric lymphoma: comparison with conventional imaging. Eur J Nucl Med Mol Imaging. 2011;38:274–84.
68. Furth C, Steffen IG, Amthauer H, et al. Early and late therapy response assessment with [^{18}F] fluorodeoxyglucose positron emission tomography in pediatric Hodgkin's lymphoma: analysis of a prospective multicenter trial. J Clin Oncol. 2009;27:4385–91.
69. Furth C, Meseck RM, Steffen IG, et al. SUV-measurements and patient-specific corrections in pediatric Hodgkin-lymphoma: is there a benefit for PPV in early response assessment by FDG-PET? Pediatr Blood Cancer. 2012;59:475–80.
70. Lyons K, Seghers V, Sorensen JI, et al. Comparison of standardized uptake values in normal structures between PET/CT and PET/MRI in a tertiary pediatric hospital: a prospective study. Am J Roentgenol. 2015;205:1094–101.
71. Hirsch FW, Sattler B, Sorge I, et al. PET/MR in children. Initial clinical experience in paediatric oncology using an integrated PET/MR scanner. Pediatr Radiol. 2013;43:860–75.
72. Punwani S, Taylor SA, Saad ZZ, et al. Diffusion-weighted MRI of lymphoma: prognostic utility and implications for PET/MRI? Eur J Nucl Med Mol Imaging. 2013;40:373–85.
73. Afaq A, Fraioli F, Sidhu H, et al. Comparison of PET/MRI with PET/CT in the evaluation of disease status in lymphoma. Clin Nucl Med. 2017;42:e1–7.
74. Radbruch A, Weberling LD, Kieslich PJ, et al. Gadolinium retention in the dentate nucleus and globus pallidus is dependent on the class of contrast agent. Radiology. 2015;275:783–91.
75. Kirchner J, Deuschl C, Schweiger B, et al. Imaging children suffering from lymphoma: an evaluation of different ^{18}F-FDG PET/MRI protocols compared to whole-body DW-MRI. Eur J Nucl Med Mol Imaging. 2017;44:1742.
76. American Cancer Society. Cancer facts & figures 2017. Atlanta: American Cancer Society; 2017.
77. Louis DN, Perry A, Reifenberger G, et al. The 2016 World Health Organization classification of tumors of the central nervous system: a summary. Acta Neuropathol. 2016;131:803–20.
78. Calcagni ML, Galli G, Giordano A, et al. Dynamic O-(2-[^{18}F]fluoroethyl)-L-tyrosine (F-18 FET) PET for glioma grading: assessment of individual probability of malignancy. Clin Nucl Med. 2011;36:841–7.
79. Popperl G, Kreth FW, Mehrkens JH, et al. FET PET for the evaluation of untreated gliomas: correlation of FET uptake and uptake kinetics with tumour grading. Eur J Nucl Med Mol Imaging. 2007;34:1933–42.
80. Pöpperl G, Kreth FW, Herms J, et al. Analysis of ^{18}F-FET PET for grading of recurrent gliomas: is evaluation of uptake kinetics superior to standard methods? J Nucl Med. 2006;47:393–403.
81. Galldiks N, Rapp M, Stoffels G, Dunkl V, Sabel M, Langen KJ. Earlier diagnosis of progressive disease during bevacizumab treatment using O-(2-^{18}F-fluorethyl)-L-tyrosine positron emission tomography in comparison with magnetic resonance imaging. Mol Imaging. 2013;12:273–6.

82. Galldiks N, Stoffels G, Filss CP, et al. Role of O-(2-^{18}F-fluoroethyl)-L-tyrosine PET for differentiation of local recurrent brain metastasis from radiation necrosis. J Nucl Med. 2012;53:1367–74.
83. Zukotynski K, Fahey F, Kocak M, et al. ^{18}F-FDG PET and MR imaging associations across a spectrum of pediatric brain tumors: a report from the pediatric brain tumor consortium. J Nucl Med. 2014;55:1473–80.
84. Patil S, Biassoni L, Borgwardt L. Nuclear medicine in pediatric neurology and neurosurgery: epilepsy and brain tumors. Semin Nucl Med. 2007;37:357–81.
85. Pirotte BJ, Lubansu A, Massager N, et al. Clinical impact of integrating positron emission tomography during surgery in 85 children with brain tumors. J Neurosurg Pediatr. 2010;5(5):486–99.
86. Pirotte BJ, Lubansu A, Massager N, Wikler D, Goldman S, Levivier M. Results of positron emission tomography guidance and reassessment of the utility of and indications for stereotactic biopsy in children with infiltrative brainstem tumors. J Neurosurg. 2007;107:392–9.
87. Torrens M, Malamitsi J, Karaiskos P, et al. Although non-diagnostic between necrosis and recurrence, FDG PET/CT assists management of brain tumours after radiosurgery. In Vivo. 2016;30:513–20.
88. Tan H, Chen L, Guan Y, Lin X. Comparison of MRI, F-18 FDG, and ^{11}C-choline PET/CT for their potentials in differentiating brain tumor recurrence from brain tumor necrosis following radiotherapy. Clin Nucl Med. 2011;36:978–81.
89. Hustinx R, Pourdehnad M, Kaschten B, Alavi A. PET imaging for differentiating recurrent brain tumor from radiation necrosis. Radiol Clin N Am. 2005;43:35–47.
90. Dankbaar JW, Snijders TJ, Robe PA, et al. The use of ^{18}F-FDG PET to differentiate progressive disease from treatment induced necrosis in high grade glioma. J Neuro-Oncol. 2015;125:167–75.
91. Nihashi T, Dahabreh IJ, Terasawa T. Diagnostic accuracy of PET for recurrent glioma diagnosis: a meta-analysis. Am J Neuroradiol. 2013;34:944–50. S1–11
92. Haining Z, Kawai N, Miyake K, et al. Relation of LAT1/4F2hc expression with pathological grade, proliferation and angiogenesis in human gliomas. BMC Clin Pathol. 2012;12:4.
93. Nawashiro H, Otani N, Shinomiya N, et al. L-type amino acid transporter 1 as a potential molecular target in human astrocytic tumors. Int J Cancer. 2006;119:484–92.
94. Nawashiro H, Otani N, Uozumi Y, et al. High expression of L-type amino acid transporter 1 in infiltrating glioma cells. Brain Tumor Pathol. 2005;22:89–91.
95. Suchorska B, Jansen NL, Linn J, et al. Biological tumor volume in ^{18}FET-PET before radiochemotherapy correlates with survival in GBM. Neurology. 2015;84:710–9.
96. Kratochwil C, Combs SE, Leotta K, et al. Intra-individual comparison of ^{18}F-FET and ^{18}F-DOPA in PET imaging of recurrent brain tumors. Neuro-Oncology. 2014;16:434–40.
97. Pauleit D, Stoffels G, Bachofner A, et al. Comparison of ^{18}F-FET and ^{18}F-FDG PET in brain tumors. Nucl Med Biol. 2009;36:779–87.
98. Miyake K, Shinomiya A, Okada M, Hatakeyama T, Kawai N, Tamiya T. Usefulness of FDG, MET and FLT-PET studies for the management of human gliomas. J Biomed Biotechnol. 2012;2012:205818.
99. Galldiks N, Ullrich R, Schroeter M, Fink GR, Kracht LW. Volumetry of [^{11}C]-methionine PET uptake and MRI contrast enhancement in patients with recurrent glioblastoma multiforme. Eur J Nucl Med Mol Imaging. 2009;37:84.
100. Juhasz C, Dwivedi S, Kamson DO, Michelhaugh SK, Mittal S. Comparison of amino acid positron emission tomographic radiotracers for molecular imaging of primary and metastatic brain tumors. Mol Imaging. 2014;13:7290201400015.
101. Grosu AL, Astner ST, Riedel E, et al. An interindividual comparison of O-(2-[^{18}F]fluoroethyl)-L-tyrosine (FET)- and L-[methyl-^{11}C]methionine (MET)-PET in patients with brain gliomas and metastases. Int J Radiat Oncol Biol Phys. 2011;81:1049–58.
102. Becherer A, Karanikas G, Szabo M, et al. Brain tumour imaging with PET: a comparison between [^{18}F]fluorodopa and [^{11}C]methionine. Eur J Nucl Med Mol Imaging. 2003;30:1561–7.

103. Pirotte B, Levivier M, Morelli D, et al. Positron emission tomography for the early postsurgical evaluation of pediatric brain tumors. Childs Nerv Syst. 2005;21:294–300.
104. Pirotte B, Goldman S, Van Bogaert P, et al. Integration of [^{11}C]methionine-positron emission tomographic and magnetic resonance imaging for image-guided surgical resection of infiltrative low-grade brain tumors in children. Neurosurgery. 2005;57:128–39. discussion 128–139
105. Pirotte B, Goldman S, Dewitte O, et al. Integrated positron emission tomography and magnetic resonance imaging-guided resection of brain tumors: a report of 103 consecutive procedures. J Neurosurg. 2006;104:238–53.
106. Misch M, Guggemos A, Driever PH, et al. ^{18}F-FET-PET guided surgical biopsy and resection in children and adolescence with brain tumors. Childs Nerv Syst. 2015;31:261–7.
107. Preuss M, Werner P, Barthel H, et al. Integrated PET/MRI for planning navigated biopsies in pediatric brain tumors. Childs Nerv Syst. 2014;30:1399–403.
108. Gauvain K, Ponisio MR, Barone A, et al. ^{18}F-FDOPA PET/MRI for monitoring early response to bevacizumab in children with recurrent brain tumors: initial experience Neuro-Oncology Pract. 2017. https://doi.org/10.1093/nop/npx008.
109. Bakhshi S, Radhakrishnan V. Prognostic markers in osteosarcoma. Expert Rev Anticancer Ther. 2010;10:271–87.
110. Crist WM, Anderson JR, Meza JL, et al. Intergroup rhabdomyosarcoma study-IV: results for patients with nonmetastatic disease. J Clin Oncol. 2001;19:3091–102.
111. Gorlick R, Janeway K, Lessnick S, Randall RL, Marina N, Committee COGBT. Children's oncology group's 2013 blueprint for research: bone tumors. Pediatr Blood Cancer. 2013;60:1009–15.
112. Bacci G, Ferrari S, Bertoni F, et al. Prognostic factors in nonmetastatic Ewing's sarcoma of bone treated with adjuvant chemotherapy: analysis of 359 patients at the Istituto Ortopedico Rizzoli. J Clin Oncol. 2000;18:4–11.
113. Sung L, Anderson JR, Donaldson SS, et al. Late events occurring five years or more after successful therapy for childhood rhabdomyosarcoma: a report from the soft tissue sarcoma committee of the Children's oncology group. Eur J Cancer. 2004;40:1878–85.
114. Rodeberg DA, Garcia-Henriquez N, Lyden ER, et al. Prognostic significance and tumor biology of regional lymph node disease in patients with rhabdomyosarcoma: a report from the Children's oncology group. J Clin Oncol. 2011;29:1304–11.
115. van Geel AN, Wyrdeman HK, Seynaeve C, et al. Practice guideline 'Diagnostic techniques for soft tissue tumours and treatment of soft tissue sarcomas (revision)'. Ned Tijdschr Geneeskd. 2005;149:924–8.
116. Brisse H, Ollivier L, Edeline V, et al. Imaging of malignant tumours of the long bones in children: monitoring response to neoadjuvant chemotherapy and preoperative assessment. Pediatr Radiol. 2004;34:595–605.
117. Pan G, Raymond AK, Carrasco CH, et al. Osteosarcoma: MR imaging after preoperative chemotherapy. Radiology. 1990;174:517–26.
118. Marina N, Gebhardt M, Teot L, Gorlick R. Biology and therapeutic advances for pediatric osteosarcoma. Oncologist. 2004;9:422–41.
119. Kellenberger CJ, Miller SF, Khan M, Gilday DL, Weitzman S, Babyn PS. Initial experience with FSE STIR whole-body MR imaging for staging lymphoma in children. Eur Radiol. 2004;14:1829–41.
120. Daldrup-Link HE, Franzius C, Link TM, et al. Whole-body MR imaging for detection of bone metastases in children and young adults: comparison with skeletal scintigraphy and FDG PET. Am J Roentgenol. 2001;177:229–36.
121. Weiser DA, Kaste SC, Siegel MJ, Adamson PC. Imaging in childhood cancer: a Society for Pediatric Radiology and Children's oncology group joint task force report. Pediatr Blood Cancer. 2013;60:1253–60.
122. Kneisl JS, Patt JC, Johnson JC, Zuger JH. Is PET useful in detecting occult nonpulmonary metastases in pediatric bone sarcomas? Clin Orthop Relat Res. 2006;450:101–4.
123. Ricard F, Cimarelli S, Deshayes E, Mognetti T, Thiesse P, Giammarile F. Additional benefit of F-18 FDG PET/CT in the staging and follow-up of pediatric rhabdomyosarcoma. Clin Nucl Med. 2011;36:672–7.

124. Buchbender C, Heusner TA, Lauenstein TC, Bockisch A, Antoch G. Oncologic PET/MRI, part 2: bone tumors, soft-tissue tumors, melanoma, and lymphoma. J Nucl Med. 2012;53:1244–52.
125. London K, Stege C, Cross S, et al. ^{18}F-FDG PET/CT compared to conventional imaging modalities in pediatric primary bone tumors. Pediatr Radiol. 2012;42:418–30.
126. Quartuccio N, Fox J, Kuk D, et al. Pediatric bone sarcoma: diagnostic performance of ^{18}F-FDG PET/CT versus conventional imaging for initial staging and follow-up. Am J Roentgenol. 2015;204:153–60.
127. Denecke T, Hundsdorfer P, Misch D, et al. Assessment of histological response of paediatric bone sarcomas using FDG PET in comparison to morphological volume measurement and standardized MRI parameters. Eur J Nucl Med Mol Imaging. 2010;37:1842–53.
128. Franzius C, Bielack S, Flege S, Sciuk J, Jurgens H, Schober O. Prognostic significance of ^{18}F-FDG and ^{99m}Tc-methylene diphosphonate uptake in primary osteosarcoma. J Nucl Med. 2002;43:1012–7.
129. Pfluger T, Melzer HI, Mueller WP, et al. Diagnostic value of combined ^{18}F-FDG PET/MRI for staging and restaging in paediatric oncology. Eur J Nucl Med Mol Imaging. 2012;39:1745–55.
130. Parodi S, Haupt R. The epidemiology of neuroblastoma. New York: Nova Biomedical; 2009.
131. Gutierrez JC, Fischer AC, Sola JE, Perez EA, Koniaris LG. Markedly improving survival of neuroblastoma: a 30-year analysis of 1,646 patients. Pediatr Surg Int. 2007;23:637–46.
132. Matthay KK, Maris JM, Schleiermacher G, et al. Neuroblastoma. Nat Rev Dis Prim. 2016;2:16078.
133. Maris JM, Hogarty MD, Bagatell R, Cohn SL. Neuroblastoma. Lancet. 2007;369:2106–20.
134. Servaes S, Epelman M, Pollock A, Shekdar K. Pediatric malignancies: synopsis of current imaging techniques. Cancer Treat Res. 2008;143:469–91.
135. Sharp SE, Parisi MT, Gelfand MJ, Yanik GA, Shulkin BL. Functional-metabolic imaging of neuroblastoma. Q J Nucl Med Mol Imaging. 2013;57:6–20.
136. Conte M, De Bernardi B, Milanaccio C, et al. Malignant neuroblastic tumors in adolescents. Cancer Lett. 2005;228:271–4.
137. Modak S, Cheung NK. Neuroblastoma: therapeutic strategies for a clinical enigma. Cancer Treat Rev. 2010;36:307–17.
138. Goo HW. Whole-body MRI of neuroblastoma. Eur J Radiol. 2010;75:306–14.
139. Goo HW, Choi SH, Ghim T, Moon HN, Seo JJ. Whole-body MRI of paediatric malignant tumours: comparison with conventional oncological imaging methods. Pediatr Radiol. 2005;35:766–73.
140. Mueller WP, Coppenrath E, Pfluger T. Nuclear medicine and multimodality imaging of pediatric neuroblastoma. Pediatr Radiol. 2013;43:418–27.
141. Lopci E, Piccardo A, Nanni C, et al. ^{18}F-DOPA PET/CT in neuroblastoma: comparison of conventional imaging with CT/MR. Clin Nucl Med. 2012;37:e73–8.
142. Piccardo A, Lopci E, Conte M, et al. Comparison of ^{18}F-dopa PET/CT and ^{123}I-MIBG scintigraphy in stage 3 and 4 neuroblastoma: a pilot study. Eur J Nucl Med Mol Imaging. 2012;39:57–71.
143. Ambrosini V, Morigi JJ, Nanni C, Castellucci P, Fanti S. Current status of PET imaging of neuroendocrine tumours ([^{18}F]FDOPA, [^{68}Ga]tracers, [^{11}C]/[^{18}F]-HTP). Q J Nucl Med Mol Imaging. 2015;59:58–69.
144. Brodeur GM, Pritchard J, Berthold F, et al. Revisions of the international criteria for neuroblastoma diagnosis, staging, and response to treatment. J Clin Oncol. 1993;11:1466–77.
145. Kushner BH. Neuroblastoma: a disease requiring a multitude of imaging studies. J Nucl Med. 2004;45:1172–88.
146. Taggart DR, Han MM, Quach A, et al. Comparison of iodine-123 metaiodobenzylguanidine (MIBG) scan and [^{18}F]fluorodeoxyglucose positron emission tomography to evaluate response after iodine-131 MIBG therapy for relapsed neuroblastoma. J Clin Oncol. 2009;27:5343–9.
147. Sharp SE, Shulkin BL, Gelfand MJ, Salisbury S, Furman WL. ^{123}I-MIBG scintigraphy and ^{18}F-FDG PET in neuroblastoma. J Nucl Med. 2009;50:1237–43.
148. Stauss J, Franzius C, Pfluger T, et al. Guidelines for ^{18}F-FDG PET and PET-CT imaging in paediatric oncology. Eur J Nucl Med Mol Imaging. 2008;35:1581–8.

149. Uslu L, Donig J, Link M, Rosenberg J, Quon A, Daldrup-Link HE. Value of ^{18}F-FDG PET and PET/CT for evaluation of pediatric malignancies. J Nucl Med. 2015;56:274–86.
150. Shulkin BL, Hutchinson RJ, Castle VP, Yanik GA, Shapiro B, Sisson JC. Neuroblastoma: positron emission tomography with 2-[fluorine-18]-fluoro-2-deoxy-D-glucose compared with metaiodobenzylguanidine scintigraphy. Radiology. 1996;199:743–50.
151. Georgantzi K, Tsolakis AV, Stridsberg M, Jakobson A, Christofferson R, Janson ET. Differentiated expression of somatostatin receptor subtypes in experimental models and clinical neuroblastoma. Pediatr Blood Cancer. 2011;56:584–9.
152. Maggi M, Baldi E, Finetti G, et al. Identification, characterization, and biological activity of somatostatin receptors in human neuroblastoma cell lines. Cancer Res. 1994;54:124–33.
153. Kong G, Hofman MS, Murray WK, et al. Initial experience with Gallium-68 DOTA-octreotate PET/CT and peptide receptor radionuclide therapy for pediatric patients with refractory metastatic neuroblastoma. J Pediatr Hematol Oncol. 2016;38:87–96.
154. Gains JE, Bomanji JB, Fersht NL, et al. ^{177}Lu-DOTATATE molecular radiotherapy for childhood neuroblastoma. J Nucl Med. 2011;52:1041–7.
155. Lu MY, Liu YL, Chang HH, et al. Characterization of neuroblastic tumors using ^{18}F-FDOPA PET. J Nucl Med. 2013;54:42–9.